Energy-Conserving Discontinuous Galerkin Methods for the Vlasov-Ampère System with Dougherty-Fokker-Planck Collision Operator

Boyang Ye* Jingwei Hu† Chi-Wang Shu‡ Xinghui Zhong§

Abstract

This paper develops energy-preserving discontinuous Galerkin (DG) methods for the Vlasov-Ampère (VA) system coupled with the Dougherty-Fokker-Planck (DFP) collision operator. While the classical VA system has been extensively studied, the inclusion of the collision operator introduces new challenges in conserving the total energy of the system. To address this, we design two energy-conserving temporal discretization methods: a second-order explicit scheme and a second-order implicit-explicit (IMEX) scheme. These schemes are coupled with the DG method, specifically using the local DG (LDG) method for the DFP part. We prove that the fully discrete schemes conserve the total particle number and total energy of the VA-DFP system at the fully discrete level. We further establish the L^2 stability of the fully discrete explicit scheme. Numerical experiments are conducted to assess the accuracy, conservation property, and performance of the proposed schemes.

Keywords: Vlasov-Ampère equation, Dougherty-Fokker-Planck operator, Energy conservation, Local discontinuous Galerkin method, Landau damping, Two-stream instability, Bump-on-tail instability.

*School of Mathematical Sciences, Zhejiang University, Hangzhou, Zhejiang 310058, P.R. China. Email: 11935020@zju.edu.cn.

†Department of Applied Mathematics, University of Washington, Seattle, WA 98195, USA. Email: hujw@uw.edu.

‡Division of Applied Mathematics, Brown University, Providence, RI 02912, USA. Email: chi-wang_shu@brown.edu.

§School of Mathematical Sciences, Zhejiang University, Hangzhou, Zhejiang 310058, P.R. China. Email: zhongxh@zju.edu.cn.

1 Introduction

The study of plasma, an ionized state of matter that plays a crucial role in various scientific fields such as space physics and fusion energy, has always been a focal point in mathematical modeling. In plasma physics, one of the fundamental mathematical representations is the Vlasov-Ampère (VA) system, which describes the time evolution of the electron distribution function, capturing the behavior of charged particles in a plasma. When coupled with the Dougherty-Fokker-Planck (DFP) collision operator [23], the VA equation becomes an essential model for studying plasma dynamics. In this paper, we present a novel approach for solving the VA system with the DFP operator, the VA-DFP system, with energy-conserving numerical schemes.

After non-dimensionalization, the VA-DFP system is given by

$$\partial_t f + \mathbf{v}\cdot\nabla_{\mathbf{x}} f + \mathbf{E}\cdot\nabla_{\mathbf{v}} f = \nu Q(f), \qquad (\mathbf{x},\mathbf{v})\in\Omega=\Omega_{\mathbf{x}}\times\Omega_{\mathbf{v}}, \tag{1.1a}$$

$$\partial_t \mathbf{E} = -\mathbf{J} = -\int_{\Omega_{\mathbf{v}}} \mathbf{v} f \,\mathrm{d}\mathbf{v}, \tag{1.1b}$$

where $f(t,\mathbf{x},\mathbf{v})$ is the probability density function of electrons at position $\mathbf{x}$ with velocity $\mathbf{v}$ at time t, and the electric field $\mathbf{E}$ is driven by the current density $\mathbf{J}$. The constant ν represents the collision frequency. The DFP collision operator, denoted by $Q(f)$, models the effects of Coulomb collisions on the particle distribution. It is given by

$$Q(f) = \nabla_{\mathbf{v}}\cdot\left(T\nabla_{\mathbf{v}} f + (\mathbf{v}-\mathbf{u})f\right), \tag{1.2}$$

with the density ρ, the average velocity $\mathbf{u}$, and the temperature T defined as

$$\rho = \int_{\Omega_{\mathbf{v}}} f \,\mathrm{d}\mathbf{v}, \quad \mathbf{u} = \frac{\mathbf{J}}{\rho}, \quad T = \frac{1}{\rho d}\int_{\Omega_{\mathbf{v}}} |\mathbf{v}-\mathbf{u}|^2 f \,\mathrm{d}\mathbf{v}, \tag{1.3}$$

where d represents the number of dimensions.[R2] The VA-DFP system is defined on the domain $\Omega = \Omega_{\mathbf{x}}\times\Omega_{\mathbf{v}}$, where $\Omega_{\mathbf{x}}$ denotes the physical domain and $\Omega_{\mathbf{v}} = \mathbb{R}^d$ represents the velocity domain. The boundary conditions are assumed to be periodic in $\mathbf{x}$ for simplicity and $f\to 0$ for $|\mathbf{v}|\to\infty$. It is worth mentioning that in practice, $\Omega_{\mathbf{v}}$ is truncated to a finite region taken large enough such that the solution $f\approx 0$ at $\partial\Omega_{\mathbf{v}}$.

It can be verified that the DFP operator conserves the ~~mass~~[R2] particle number[R2], momentum, and energy

$$\int_{\Omega_{\mathbf{v}}} Q(f)\,\mathrm{d}\mathbf{v} = \int_{\Omega_{\mathbf{v}}} \mathbf{v} Q(f)\,\mathrm{d}\mathbf{v} = \int_{\Omega_{\mathbf{v}}} \frac{|\mathbf{v}|^2}{2} Q(f)\,\mathrm{d}\mathbf{v} = 0. \tag{1.4}$$

The VA-DFP system (1.1) conserves the total particle number $\int_\Omega f\,\mathrm{d}\mathbf{x}\,\mathrm{d}\mathbf{v}$, and the total energy

$$TE = \iint_{\Omega_{\mathbf{x}}\times\Omega_{\mathbf{v}}} \frac{1}{2}|\mathbf{v}|^2 f \,\mathrm{d}\mathbf{v}\,\mathrm{d}\mathbf{x} + \frac{1}{2}\int_{\Omega_{\mathbf{x}}} |\mathbf{E}|^2 \,\mathrm{d}\mathbf{x}, \tag{1.5}$$

which consists of the kinetic energy and electric energy.

When the collision frequency ν is zero, the VA-DFP system (1.1) simplifies to the classical VA system, which is regarded as the zero-magnetic limit of the Vlasov-Maxwell (VM) system and is also equivalent to the Vlasov-Poisson (VP) system under certain conditions. In the context of Vlasov solvers, one approach is the popular particle-in-cell (PIC) methods [36, 6, 7], which involve advancing macro-particles in a Lagrangian framework, while solving the field equations using mesh-based methods. Another approach is the deterministic solvers, which directly compute solutions under an Eulerian or semi-Lagrangian framework. These solvers have gained attention for their ability to provide highly accurate results without introducing statistical noise. Works in this approach include semi-Lagrangian methods [8, 50, 51, 49, 52, 46, 22, 47, 48, 5, 43], the weighted essentially non-oscillatory (WENO) method coupled with Fourier collocation [63], finite volume methods [28, 29, 25, 15, 56, 55], a spectral element method [44], Fourier-Fourier spectral methods [39, 40], continuous finite element methods [58, 59], and Runge–Kutta (RK) discontinuous Galerkin (DG) methods [3, 4, 13, 34, 33], among others.

One of the main challenges for Vlasov solvers is the conservation of macroscopic quantities, such as the total particle number and total energy. While most Vlasov methods maintain particle number conservation, energy conservation is often overlooked, resulting in unphysical outcomes such as plasma self-heating or cooling. Energy-conserving PIC methods were proposed for the VA system in [7] and for the VM system in [45]. Energy-conserving finite difference method was proposed for VP system in [29]. Energy-conserving semi-Lagrangian methods was proposed for the VA system in [43]. Energy-conserving moment method was proposed for the multi-dimensional VM system in [57]. Energy-conserving DG spectral element method was proposed for the VP system in [44]. Energy-conserving DG scheme at the semi-discrete level was proposed for the VP system in [3, 4] and for the VM system in [14]. Energy-conserving DG schemes at the fully discrete level were proposed for the VA system in [9], for the VM system in [10], and for the two-species VA system in [11, 12].

In this paper, we focus on the VA-DFP system, where the incorporation of the collision term $Q(f)$ introduces new challenges and complexities. Typically, Coulomb collisions in a plasma are described by the Landau operator [41], which is an integro-differential operator. The DFP operator [23], also known as the ~~Lenard-Bernstain~~[R2] Lenard-Bernstein[R2] operator [42], can be considered as a simplified Landau operator that conserves particle number, momentum, and energy, as well as decays entropy. It correctly models the behavior of most particles in a thermal distribution, despite inaccuracies in the high-energy tail. A system governed solely by the DFP operator, namely $f_t = Q(f)$, will eventually converge to a steady state characterized by a Maxwellian function.[R2] This operator has been studied in numerical methods including finite volume methods [53, 54], recovery DG methods [26, 32] and sta-

bilized RK methods [1]. For numerical methods of other Fokker-Planck-type operators, see [2, 27, 30, 60, 38] for an incomplete list.

The main objective of this paper is to develop energy-conserving DG methods for the VA-DFP system (1.1) *at the fully discrete level*. Building upon the energy-conserving methods proposed for the VA system in [9], we design two energy-conserving temporal discretization methods with additional care taken for the DFP operator. The first method is a second-order explicit scheme that balances the kinetic and electric energies. The second method is a second-order implicit-explicit (IMEX) scheme that treats the Vlasov part explicitly and the DFP part implicitly, allowing for a relaxation of the CFL restriction on the time step size and enhancing computational efficiency. For the discretization in the phase space, we employ the DG methods [17, 18, 19, 20], which are a class of finite element methods that employ discontinuous piecewise polynomial spaces for both the numerical solution and test functions. In particular, for the DFP part involving second-order derivatives, we employ the local DG (LDG) methods [21], which rewrites the second-order equations as an equivalent first-order system and then applies the DG method. The LDG method inherits many advantages of the DG methods including the capability in *h-p* adaptivity, the ability to handle arbitrary triangulations, efficient parallel implementation, and the ability of handling complicated boundary conditions and curved interface. We prove that the two fully discrete schemes conserve the total particle number and total energy of the VA-DFP system. Furthermore, we establish the L^2 stability of the fully discrete explicit scheme. Numerical experiments are carried out to test the accuracy, conservation properties, and performance of the proposed schemes. Compared to recovery DG methods in[R2] [26, 32], the LDG method avoids the need for global recovery of derivatives. Thus it is simpler to implement and exhibits better efficiency. Moreover, the LDG method offers theoretical stability and can be easily extended to high-dimensional cases.[R2]

The paper is organized as follows: In Section 2, we introduce two second-order time discretizations that conserve the total particle number and total energy. In Section 3, we discuss the fully discrete schemes by using the DG methods for discretizing phase space and establish the conservation and stability analysis. In Section 4, several numerical examples are presented to illustrate the accuracy and effectiveness of our energy-conserving schemes. We conclude the paper with some remarks in Section 5.

2 Numerical methods: temporal discretizations

In this section, we investigate two energy-conserving temporal discretization methods for the VA-DFP equation (1.1), while leaving the variables $(\mathbf{x}, \mathbf{v})$ continuous in the discussions.

Let Δt denote the time step size and $(f^n, \mathbf{E}^n)$ denote the solution at n-th time level. The

first scheme is a second-order explicit scheme designed as follows:

$$\frac{f^{n+1/2}-f^n}{\Delta t/2}+\mathbf{v}\cdot\nabla_{\mathbf{x}}f^n+\mathbf{E}^n\cdot\nabla_{\mathbf{v}}f^n=\nu Q(f^n), \tag{2.1a}$$

$$\frac{\mathbf{E}^{n+1}-\mathbf{E}^n}{\Delta t}=-\mathbf{J}^{n+1/2},\quad \mathbf{J}^{n+1/2}=\int_{\Omega_{\mathbf{v}}}\mathbf{v}f^{n+1/2}\,\mathrm{d}\mathbf{v}, \tag{2.1b}$$

$$\frac{f^{n+1}-f^n}{\Delta t}+\mathbf{v}\cdot\nabla_{\mathbf{x}}f^{n+1/2}+\left(\frac{\mathbf{E}^n+\mathbf{E}^{n+1}}{2}\right)\cdot\nabla_{\mathbf{v}}f^{n+1/2}=\nu Q(f^{n+1/2}). \tag{2.1c}$$

This scheme is constructed by carefully coupling the Vlasov and Ampère solvers to balance the kinetic and electric energies. This scheme conserves the total particle number and total energy, as stated in Theorems 2.1 and 2.2. However, as an explicit scheme, it suffers from the CFL restriction, especially from the DFP term.

To relax the CFL restriction on the time step size and improve the efficiency, we modify the first scheme by using a second-order IMEX method that treats the Vlasov part explicitly and the DFP part implicitly:

$$\frac{f^{n+1/2}-f^n}{\Delta t/2}+\mathbf{v}\cdot\nabla_{\mathbf{x}}f^n+\mathbf{E}^n\cdot\nabla_{\mathbf{v}}f^n=\nu Q(f^{n+1/2}), \tag{2.2a}$$

$$\frac{\mathbf{E}^{n+1}-\mathbf{E}^n}{\Delta t}=-\mathbf{J}^{n+1/2},\quad \mathbf{J}^{n+1/2}=\int_{\Omega_{\mathbf{v}}}\mathbf{v}f^{n+1/2}\,\mathrm{d}\mathbf{v}, \tag{2.2b}$$

$$\frac{f^{n+1}-f^n}{\Delta t}+\mathbf{v}\cdot\nabla_{\mathbf{x}}f^{n+1/2}+\left(\frac{\mathbf{E}^n+\mathbf{E}^{n+1}}{2}\right)\cdot\nabla_{\mathbf{v}}f^{n+1/2}=\frac{\nu}{2}Q(f^n)+\frac{\nu}{2}Q(f^{n+1}). \tag{2.2c}$$

Although the nonlinear collision term appears fully implicitly in (2.2a) and (2.2c), they can be implemented efficiently as follows. Take Equation (2.2a) as an example. By applying the operation $\int_{\Omega_{\mathbf{v}}}\cdot(1,\mathbf{v},|\mathbf{v}|^2/2)^T\,\mathrm{d}\mathbf{v}$ to both sides of the equation, together with the conservation properties of the DFP operator in (1.4), we have

$$\frac{\mathbf{U}^{n+1/2}-\mathbf{U}^n}{\Delta t/2}+\int_{\Omega_{\mathbf{v}}}(\mathbf{v}\cdot\nabla_{\mathbf{x}}f^n+\mathbf{E}^n\cdot\nabla_{\mathbf{v}}f^n)(1,\mathbf{v},|\mathbf{v}|^2/2)^T\,\mathrm{d}\mathbf{v}=0, \tag{2.3}$$

where $\mathbf{U}:=(\rho,\rho\mathbf{u},\frac{1}{2}\rho|\mathbf{u}|^2+\rho\frac{d}{2}T)^T$. Clearly $\mathbf{U}^{n+1/2}$ can be explicitly determined from $(f^n,\mathbf{E}^n)$, which consequently determines $\mathbf{u}^{n+1/2}$ and $T^{n+1/2}$. Thus the implicit DFP operator $Q(f^{n+1/2})$ is linear in $f^{n+1/2}$, and $f^{n+1/2}$ can be solved by an implicit linear solver. Equation (2.2c) can be treated in a similar fashion.

In the following two theorems, we present the conservation properties of the above two schemes. It follows from the properties of the DFP operator in (1.4) that the conservation properties of both schemes are the same as **Scheme-1** in [9] for the VA system without the DFP operator. Therefore, the proof of the total energy conservation is similar to the proof of [9, Theorem 3.1] and is omitted here. The proof of the total partial number conservation is straightforward by the definition of the schemes and application of boundary conditions.

Theorem 2.1 (**Total particle number conservation).** Both the explicit scheme (2.1) and the IMEX scheme (2.2) conserve the total particle number of the system, i.e.,

$$\int_{\Omega_{\mathbf{x}}}\int_{\Omega_{\mathbf{v}}} f^{n+1}\,\mathrm{d}\mathbf{v}\,\mathrm{d}\mathbf{x} = \int_{\Omega_{\mathbf{x}}}\int_{\Omega_{\mathbf{v}}} f^{n}\,\mathrm{d}\mathbf{v}\,\mathrm{d}\mathbf{x}. \tag{2.4}$$

Theorem 2.2 (**Total energy conservation).** Both the explicit scheme (2.1) and the IMEX scheme (2.2) conserve the total energy of the system, i.e.,

$$\int_{\Omega_{\mathbf{x}}}\int_{\Omega_{\mathbf{v}}} \frac{|\mathbf{v}|^2}{2} f^{n+1}\,\mathrm{d}\mathbf{v}\,\mathrm{d}\mathbf{x} + \int_{\Omega_{\mathbf{x}}} \frac{|\mathbf{E}^{n+1}|^2}{2}\,\mathrm{d}\mathbf{x} = \int_{\Omega_{\mathbf{x}}}\int_{\Omega_{\mathbf{v}}} \frac{|\mathbf{v}|^2}{2} f^{n}\,\mathrm{d}\mathbf{v}\,\mathrm{d}\mathbf{x} + \int_{\Omega_{\mathbf{x}}} \frac{|\mathbf{E}^{n}|^2}{2}\,\mathrm{d}\mathbf{x}. \tag{2.5}$$

Remark 2.1. In addition to the good conservation property, the IMEX scheme (2.2) is also asymptotic-preserving (AP). Specifically, when the initial condition is at equilibrium, as the collision frequency $\nu \to \infty$, this scheme will become a second-order explicit scheme applied to the limiting fluid model (in this case, the Euler-Ampère system). Readers can refer to [37] (scheme IMEX-II-GSA(2,3,2)) for more details.

3 Numerical methods: fully discrete methods

In this section, we formulate the fully discrete schemes by using the DG methods to discretize the $(\mathbf{x}, \mathbf{v})$ variables, and discuss their conservation and stability properties. For simplicity of discussion, we focus on the schemes in a 1D1V setting as an illustrative example to show the main idea. The system (1.1) under 1D1V setting is given by

$$f_t + v f_x + E f_v = \nu Q(f), \tag{3.1a}$$

$$E_t = -J, \tag{3.1b}$$

where $Q(f) = T f_{vv} + ((v-u)f)_v$ with T and u defined in (1.3) under 1D setting.

3.1 Fully discrete scheme with the DG method

In this section, we present the DG method coupling with the time integrators introduced in Section 2 to formulate the fully discrete schemes.

We start by making a uniform partition of the domain Ω, consisting of cells of $K_{ij} = [x_{i-\frac{1}{2}}, x_{i+\frac{1}{2}}] \times [v_{j-\frac{1}{2}}, v_{j+\frac{1}{2}}]$ for $1 \leqslant i \leqslant N_x$ and $1 \leqslant j \leqslant N_v$, with the mesh size as $\Delta x = x_{i+\frac{1}{2}} - x_{i-\frac{1}{2}}$ and $\Delta v = v_{j+\frac{1}{2}} - v_{j-\frac{1}{2}}$. The uniform mesh is adopted to simplify the presentation, and our results hold for general cartesian meshes. We further define $I_i = [x_{i-\frac{1}{2}}, x_{i+\frac{1}{2}}]$ and $J_j = [v_{j-\frac{1}{2}}, v_{j+\frac{1}{2}}]$. The finite element approximation space is defined by

$$\mathbb{V}_h^k := \{\zeta : \zeta|_{K_{ij}} \in P^k(K_{ij}),\ \ 1 \leqslant i \leqslant N_x,\ 1 \leqslant j \leqslant N_v\},$$

where $P^k(K_{ij})$ denotes the set of polynomials of total degree up to k on cell K_{ij}. We also introduce the following notations to simplify the presentation of the DG scheme

$$(f,g)_{K_{ij}} = \int_{K_{ij}} fg \,\mathrm{d}x\,\mathrm{d}v, \quad \langle f,g\rangle_{I_i} = \int_{I_i} fg \,\mathrm{d}x, \quad \langle f,g\rangle_{J_j} = \int_{J_j} fg \,\mathrm{d}v. \tag{3.2}$$

To define the DG method for the system containing second-order derivatives, we first rewrite (3.1) as an equivalent first-order system

$$f_t + vf_x + Ef_v = \nu\left(p_v + ((v-u)f)_v\right), \tag{3.3a}$$

$$p = Tf_v, \tag{3.3b}$$

$$E_t = -J, \tag{3.3c}$$

by introducing the auxiliary variable p. With a slight abuse of notations, the DG scheme with the explicit time integrator (2.1) for solving (3.3) is defined as follows: find the unique functions $f^{n+\frac{1}{2}}, f^{n+1}, p^n, p^{n+\frac{1}{2}} \in \mathbb{V}_h^k$ such that for $i = 1,\dots,N_x,\ j = 1,\dots,N_v$,

$$\begin{aligned}
&\left(\frac{f^{n+\frac{1}{2}} - f^n}{\Delta t/2}, \phi_1\right)_{K_{ij}} - (vf^n, (\phi_1)_x)_{K_{ij}} - (E^n f^n, (\phi_1)_v)_{K_{ij}} \\
&+ \left\langle v\check{f}^n_{i+\frac{1}{2},v}, \phi_1(x^-_{i+\frac{1}{2}}, v)\right\rangle_{J_j} - \left\langle v\check{f}^n_{i-\frac{1}{2},v}, \phi_1(x^+_{i-\frac{1}{2}}, v)\right\rangle_{J_j} \\
&+ \left\langle E^n\check{f}^n_{x,j+\frac{1}{2}}, \phi_1(x, v^-_{j+\frac{1}{2}})\right\rangle_{I_i} - \left\langle E^n\check{f}^n_{x,j-\frac{1}{2}}, \phi_1(x, v^+_{j-\frac{1}{2}})\right\rangle_{I_i} = \nu\mathcal{Q}_{ij}(p^n, \phi_1),
\end{aligned} \tag{3.4a}$$

$$\frac{E^{n+1} - E^n}{\Delta t} = -J^{n+\frac{1}{2}}, \text{ with } J^{n+\frac{1}{2}} = \int_{\Omega_v} f^{n+\frac{1}{2}} v \ \mathrm{d}v, \tag{3.4b}$$

$$\begin{aligned}
&\left(\frac{f^{n+1} - f^n}{\Delta t}, \phi_2\right)_{K_{ij}} - \left(vf^{n+\frac{1}{2}}, (\phi_2)_x\right)_{K_{ij}} - \frac{1}{2}\left((E^n + E^{n+1})f^{n+\frac{1}{2}}, (\phi_2)_v\right)_{K_{ij}} \\
&+ \left\langle v\check{f}^{n+\frac{1}{2}}_{i+\frac{1}{2},v}, \phi_2(x^-_{i+\frac{1}{2}}, v)\right\rangle_{J_j} - \left\langle v\check{f}^{n+\frac{1}{2}}_{i-\frac{1}{2},v}, \phi_2(x^+_{i-\frac{1}{2}}, v)\right\rangle_{J_j} + \frac{1}{2}\left\langle (E^n + E^{n+1})\check{f}^{n+\frac{1}{2}}_{x,j+\frac{1}{2}}, \phi_2(x, v^-_{j+\frac{1}{2}})\right\rangle_{I_i} \\
&- \frac{1}{2}\left\langle (E^n + E^{n+1})\check{f}^{n+\frac{1}{2}}_{x,j-\frac{1}{2}}, \phi_2(x, v^+_{j-\frac{1}{2}})\right\rangle_{I_i} = \nu\mathcal{Q}_{ij}(p^{n+\frac{1}{2}}, \phi_2),
\end{aligned} \tag{3.4c}$$

$$(p^l, \varphi)_{K_{ij}} = \left\langle T^l\hat{f}^l_{x,j+\frac{1}{2}}, \varphi(x, v^-_{j+\frac{1}{2}})\right\rangle_{I_i} - \left\langle T^l\hat{f}^l_{x,j-\frac{1}{2}}, \varphi(x, v^+_{j-\frac{1}{2}})\right\rangle_{I_i} - (T^l f^l, \varphi_v)_{K_{ij}},\ l = n, n+\frac{1}{2}, \tag{3.4d}$$

holds for all test functions $\phi_1, \phi_2, \psi^{\mathrm{R2}}\ \varphi^{\mathrm{R2}} \in \mathbb{V}_h^k$. Here the operator $\mathcal{Q}_{ij}$ is defined as

$$\begin{aligned}
\mathcal{Q}_{ij}(p,\phi) = &-(p, \phi_v)_{K_{ij}} + \left\langle \hat{p}_{x,j+\frac{1}{2}}, \phi(x, v^-_{j+\frac{1}{2}})\right\rangle_{I_i} - \left\langle \hat{p}_{x,j-\frac{1}{2}}, \phi(x, v^+_{j-\frac{1}{2}})\right\rangle_{I_i} - ((v-u)f, \phi_v)_{K_{ij}} \\
&+ \left\langle (v_{j+\frac{1}{2}} - u)\tilde{f}_{x,j+\frac{1}{2}}, \phi(x, v^-_{j+\frac{1}{2}})\right\rangle_{I_i} - \left\langle (v_{j-\frac{1}{2}} - u)\tilde{f}_{x,j-\frac{1}{2}}, \phi(x, v^+_{j-\frac{1}{2}})\right\rangle_{I_i},
\end{aligned} \tag{3.5}$$

where both u and T are determined by applying the Gaussian quadrature rule to (1.3) with f's value obtained at the same time level as p. Specifically, denote $\{v_{j_\ell}\}_{\ell=1}^k$ as the Gaussian

quadrature points in J_j and $\{w_\ell\}_{\ell=1}^k$ as the associated quadrature weights. Then u and T can be computed by

$$u(x) = \frac{\sum_{j=1}^{N_v}\sum_{\ell=1}^{k}\omega_\ell v_{j_\ell} f(x, v_{j_\ell})}{\sum_{j=1}^{N_v}\sum_{\ell=1}^{k}\omega_\ell f(x, v_{j_\ell})}, \qquad T(x) = \frac{\sum_{j=1}^{N_v}\sum_{\ell=1}^{k}\omega_\ell (v_{j_\ell} - u(x))^2 f(x, v_{j_\ell})}{\sum_{j=1}^{N_v}\sum_{\ell=1}^{k}\omega_\ell f(x, v_{j_\ell})}. \tag{3.6}$$

The functions $\check{f}_{i+\frac{1}{2},v}$, $\check{f}_{x,j+\frac{1}{2}}$, $\hat{f}_{x,j+\frac{1}{2}}$, $\hat{p}_{x,j+\frac{1}{2}}$, and $\tilde{f}_{x,j+\frac{1}{2}}$ are the so-called numerical fluxes, which are defined at the cell interfaces. The fluxes are crucial for the accuracy, stability and conservation properties of the methods. For the Vlasov part, the fluxes in (3.4a) can be taken to be the central flux or upwind flux. It has been investigated in [9] for the VA system that the central flux causes lack of numerical dissipation, and the numerical schemes produce oscillations when filamentation occurs. Thus, the fluxes in (3.4a) are taken to be the upwind flux, given by

$$\check{f}_{i+\frac{1}{2},v} = \check{f}(x_{i+\frac{1}{2}}, v) = \begin{cases} f(x^-_{i+\frac{1}{2}}, v) & \text{, if } v \geqslant 0, \\ f(x^+_{i+\frac{1}{2}}, v) & \text{, if } v < 0, \end{cases} \tag{3.7}$$

$$\check{f}_{x,j+\frac{1}{2}} = \check{f}(x, v_{j+\frac{1}{2}}) = \begin{cases} f(x, v^-_{j+\frac{1}{2}}) & \text{, if } \overline{(E)}_{I_i} \geqslant 0, \\ f(x, v^+_{j+\frac{1}{2}}) & \text{, if } \overline{(E)}_{I_i} < 0, \end{cases} \tag{3.8}$$

where $\overline{(E)}_{I_i} = \frac{1}{\Delta x}\int_{I_i} E \,\mathrm{d}x$, x^-, x^+ are the left and right limits of x at the cell interface in the x-direction, and v^-, v^+ are the bottom and top limits of v at the cell interface in the v-direction. For the DFP part, the fluxes $\hat{f}_{x,j+\frac{1}{2}}$ and $\hat{p}_{x,j+\frac{1}{2}}$ in (3.4d)and (3.5) are taken the alternating fluxes

$$\hat{f}_{x,j+\frac{1}{2}} = \hat{f}(x, v_{j+\frac{1}{2}}) = f(x, v^-_{j+\frac{1}{2}}), \quad \hat{p}_{x,j+\frac{1}{2}} = \hat{p}(x, v_{j+\frac{1}{2}}) = p(x, v^+_{j+\frac{1}{2}}), \tag{3.9}$$

and the flux $\tilde{f}_{x,j+\frac{1}{2}}$ is taken as the upwind flux

$$\tilde{f}_{x,j+\frac{1}{2}} = \tilde{f}(x, v_{j+\frac{1}{2}}) = \begin{cases} f(x, v^-_{j+\frac{1}{2}}) & \text{, if } v_{j+\frac{1}{2}} \leqslant \overline{(u)}_{I_i}, \\ f(x, v^+_{j+\frac{1}{2}}) & \text{, if } v_{j+\frac{1}{2}} > \overline{(u)}_{I_i}, \end{cases} \tag{3.10}$$

with $\overline{(u)}_{I_i} = \frac{1}{\Delta x}\int_{I_i} u \,\mathrm{d}x$.

The fully discrete scheme with the IMEX scheme (2.2) can be formulated in a similar way.

3.2 Conservation properties

In this section, we prove the conservation properties of the proposed schemes. We first show the following lemmas which play an important role in the proof of the total energy conservation.

Lemma 3.1. The DG solution of the auxiliary variable p defined in (3.4d) satisfies

$$\int_{\Omega_x}\int_{\Omega_v} p\,\mathrm{d}x\,\mathrm{d}v = 0, \tag{3.11}$$

$$\int_{\Omega_x}\int_{\Omega_v} pv\,\mathrm{d}x\,\mathrm{d}v = -\int_{\Omega_x}\int_{\Omega_v} Tf\,\mathrm{d}x\,\mathrm{d}v. \tag{3.12}$$

Proof. By taking $\varphi(x,v)=1$ and $\varphi(x,v)=v$ in (3.4d), we have

$$\iint_{K_{ij}} p\,\mathrm{d}x\,\mathrm{d}v = \int_{I_i} T(\hat{f}_{x,j+\frac{1}{2}} - \hat{f}_{x,j-\frac{1}{2}})\,\mathrm{d}x, \tag{3.13}$$

$$\iint_{K_{ij}} pv\,\mathrm{d}x\,\mathrm{d}v = \int_{I_i} T(\hat{f}_{x,j+\frac{1}{2}} v_{j+\frac{1}{2}} - \hat{f}_{x,j-\frac{1}{2}} v_{j-\frac{1}{2}})\,\mathrm{d}x - \iint_{K_{ij}} Tf\,\mathrm{d}x\,\mathrm{d}v. \tag{3.14}$$

Then by summing up (3.13) and (3.14) over i,j, together with the boundary conditions, we complete the proof. □

Lemma 3.2. For the fully discrete schemes with P^k polynomials, the operator $\mathcal{Q}_{ij}$ defined in (3.5) satisfies the following properties

$$\sum_{i,j} \mathcal{Q}_{ij}(p,1) = 0, \tag{3.15a}$$

$$\sum_{i,j} \mathcal{Q}_{ij}(p,v) = 0, \quad \text{if } k \geqslant 1, \tag{3.15b}$$

$$\sum_{i,j} \mathcal{Q}_{ij}(p,v^2) = 0, \quad \text{if } k \geqslant 2. \tag{3.15c}$$

Proof. It follows from setting $\phi(x,v)=1$ in (3.5) that

$$\mathcal{Q}_{ij}(p,1) = \int_{I_i} \left(\hat{p}_{x,j+\frac{1}{2}} - \hat{p}_{x,j-\frac{1}{2}} + (v_{j+\frac{1}{2}} - u)\tilde{f}_{x,j+\frac{1}{2}} - (v_{j-\frac{1}{2}} - u)\tilde{f}_{x,j-\frac{1}{2}}\right)\mathrm{d}x. \tag{3.16}$$

By summing up (3.16) over i,j, and taking into account of the boundary conditions, we complete the proof of (3.15a).

If $k \geqslant 1$, we take $\phi(x,v)=v$ in (3.5). It is worth noting that $\phi(x,v)=v \in \mathbb{V}_h^k$ and is continuous. This allows us to express (3.5) as

$$\begin{aligned}\mathcal{Q}_{ij}(p,v) = &\int_{I_i} \hat{p}_{x,j+\frac{1}{2}} v_{j+\frac{1}{2}} - \hat{p}_{x,j-\frac{1}{2}} v_{j-\frac{1}{2}}\,\mathrm{d}x - \iint_{K_{ij}} p\,\mathrm{d}x\,\mathrm{d}v - \iint_{K_{ij}} (v-u) f\,\mathrm{d}x\,\mathrm{d}v \\ &+ \int_{I_i} (v_{j+\frac{1}{2}} - u)\tilde{f}_{x,j+\frac{1}{2}} v_{j+\frac{1}{2}} - (v_{j-\frac{1}{2}} - u)\tilde{f}_{x,j-\frac{1}{2}} v_{j-\frac{1}{2}}\,\mathrm{d}x.\end{aligned} \tag{3.17}$$

By summing over ~~all element K_{ij}~~[R2] i, j[R2] and utilizing Lemma 3.1, we have

$$\sum_{i,j} \mathcal{Q}_{ij}(p, v) = -\int_{\Omega_x}\int_{\Omega_v} (v-u)f \,\mathrm{d}x\,\mathrm{d}v. \tag{3.18}$$

Thus, with the definition of u in (1.3), the proof of (3.15b) is complete.

The proof of (3.15c) follows a similar approach. Since $v^2 \in \mathbb{V}_h^k$ for $k \geqslant 2$ and is continuous, we can take $\phi = v^2$ in (3.5) to obtain

$$\begin{aligned}\mathcal{Q}_{ij}(p, v^2) = &\int_{I_i} \hat{p}_{x,j+\frac{1}{2}} v_{j+\frac{1}{2}}^2 - \hat{p}_{x,j-\frac{1}{2}} v_{j-\frac{1}{2}}^2 \,\mathrm{d}x - 2\iint_{K_{ij}} pv \,\mathrm{d}x\,\mathrm{d}v - 2\iint_{K_{ij}} v(v-u)f \,\mathrm{d}x\,\mathrm{d}v \\ &+ \int_{I_i} (v_{j+\frac{1}{2}} - u)\tilde{f}_{x,j+\frac{1}{2}} v_{j+\frac{1}{2}}^2 - (v_{j-\frac{1}{2}} - u)\tilde{f}_{x,j-\frac{1}{2}} v_{j-\frac{1}{2}}^2 \,\mathrm{d}x.\end{aligned} \tag{3.19}$$

Then it follows from summing (3.19) over i, j, considering the boundary conditions, and applying Lemma 3.1 that

$$\sum_{i,j} \mathcal{Q}_{ij}(p, v^2) = -2\int_{\Omega_x}\int_{\Omega_v} v(v-u)f - Tf \,\mathrm{d}x\,\mathrm{d}v, \tag{3.20}$$

which, together with the definition of u and T in (1.3), completes the proof of (3.15c). □

Theorem 3.1 (**Total particle number conservation).** The fully discrete scheme (3.4) conserves the total particle number of the VA-DFP system, i.e.,

$$\int_{\Omega_x}\int_{\Omega_v} f^{n+1} \,\mathrm{d}x\,\mathrm{d}v = \int_{\Omega_x}\int_{\Omega_v} f^{n} \,\mathrm{d}x\,\mathrm{d}v. \tag{3.21}$$

This also holds for DG methods with the IMEX scheme (2.2) as time integrator.

Proof. The proof is straightforward by setting $\phi = 1$ in (3.4c), summing over i, j, and applying boundary conditions and Lemma 3.2. □

Theorem 3.2 (**Total energy conservation).** If $k \geqslant 2$, the fully discrete scheme (3.4) with P^k polynomial approximations conserves total energy, i.e.,

$$\frac{1}{2}\int_{\Omega_x}\int_{\Omega_v} f^{n+1}v^2 \,\mathrm{d}x\,\mathrm{d}v + \frac{1}{2}\int_{\Omega_x} (E^{n+1})^2 \,\mathrm{d}x = \frac{1}{2}\int_{\Omega_x}\int_{\Omega_v} f^{n}v^2 \,\mathrm{d}x\,\mathrm{d}v + \frac{1}{2}\int_{\Omega_x} (E^{n})^2 \,\mathrm{d}x. \tag{3.22}$$

This also holds for DG methods with the IMEX scheme (2.2) as time integrator.

Proof. By taking $\phi_2 = v^2$ in (3.4c), which belongs to the space $\mathbb{V}_h^k$ for $k \geqslant 2$ and is continuous, we have

$$\begin{aligned}&\left(\frac{f^{n+1} - f^n}{\Delta t}, v^2\right)_{K_{ij}} - \left((E^n + E^{n+1})f^{n+\frac{1}{2}}, v\right)_{K_{ij}} + \left\langle v\check{f}^{n+\frac{1}{2}}_{i+\frac{1}{2},v}, v^2\right\rangle_{J_j} - \left\langle v\check{f}^{n+\frac{1}{2}}_{i-\frac{1}{2},v}, v^2\right\rangle_{J_j} \\ &+ \frac{1}{2}\left\langle (E^n + E^{n+1})\check{f}^{n+\frac{1}{2}}_{x,j+\frac{1}{2}}, v^2_{j+\frac{1}{2}}\right\rangle_{I_i} - \frac{1}{2}\left\langle (E^n + E^{n+1})\check{f}^{n+\frac{1}{2}}_{x,j-\frac{1}{2}}, v^2_{j-\frac{1}{2}}\right\rangle_{I_i} = \nu\mathcal{Q}_{ij}(p^{n+\frac{1}{2}}, v^2).\end{aligned}$$

Then by summing over ~~all element K_{ij}~~[R2] i, j[R2] and applying boundary conditions and Lemma 3.2, we obtain

$$\int_{\Omega_x}\int_{\Omega_v}\frac{(f^{n+1}-f^n)v^2}{\Delta t}\,\mathrm{d}x\,\mathrm{d}v=\int_{\Omega_x}(E^n+E^{n+1})\left(\int_{\Omega_v}vf^{n+\frac{1}{2}}\,\mathrm{d}v\right)\mathrm{d}x,$$

which leads to

$$\int_{\Omega_x}\int_{\Omega_v}\frac{(f^{n+1}-f^n)v^2}{\Delta t}\,\mathrm{d}x\,\mathrm{d}v=\int_{\Omega_x}(E^n+E^{n+1})J^{n+\frac{1}{2}}\,\mathrm{d}x, \tag{3.23}$$

On the other hand, it follows from (3.4b) that

$$\int_{\Omega_x}(E^{n+1}+E^n)\frac{E^{n+1}-E^n}{\Delta t}\,\mathrm{d}x=-\int_{\Omega_x}(E^{n+1}+E^n)J^{n+\frac{1}{2}}\,\mathrm{d}x. \tag{3.24}$$

The proof is complete by combining (3.23) and (3.24).

The proof for the fully discrete scheme with the IMEX scheme can be conducted in a similar way. □

3.3 L^2 stability

In this section, we establish the L^2 stability for the fully discrete explicit scheme.

We introduce the bilinear operators $H^{x\pm}(r,s)(v)$ and $H^{v\pm}(r,s)(x)$ defined as follows

$$H^{x\pm}(r,s)=\sum_i\left(\langle r,s_x\rangle_{I_i}-r(x^{\pm}_{i+\frac{1}{2}},v)s(x^{-}_{i+\frac{1}{2}},v)+r(x^{\pm}_{i-\frac{1}{2}},v)s(x^{+}_{i-\frac{1}{2}},v)\right), \tag{3.25a}$$

$$H^{v\pm}(r,s)=\sum_j\left(\langle r,s_v\rangle_{J_j}-r(x,v^{\pm}_{j+\frac{1}{2}})s(x,v^{-}_{j+\frac{1}{2}})+r(x,v^{\pm}_{j-\frac{1}{2}})s(x,v^{+}_{j-\frac{1}{2}})\right), \tag{3.25b}$$

where $r,s\in\mathbb{V}_h^k$. We use $\|\cdot\|_2$ denoted as the standard L^2 norm in Ω and define the jump semi-norms as

$$[\![r]\!]_{(x)}(v)=\sqrt{\sum_i(r(x^{+}_{i+\frac{1}{2}},v)-r(x^{-}_{i+\frac{1}{2}},v))^2},\quad v\in\mathbb{V}_h^k, \tag{3.26a}$$

$$[\![r]\!]_{(v)}(x)=\sqrt{\sum_j(r(x,v^{+}_{j+\frac{1}{2}})-r(x,v^{-}_{j+\frac{1}{2}}))^2},\quad x\in\mathbb{V}_h^k. \tag{3.26b}$$

The following lemma shows the inverse property of the finite element space $\mathbb{V}_h^k$. More details can be found in [16].

Lemma 3.3. For any function $r\in\mathbb{V}_h^k$, there exists a positive constant c_1 independent of Δv such that

$$\Delta v\sqrt{\int_{\Omega_v}r_v^2\,\mathrm{d}v}+\sqrt{\Delta v\sum_j\left(r^2(x,v^{+}_{j-\frac{1}{2}})+r^2(x,v^{-}_{j+\frac{1}{2}})\right)}\leqslant c_1\sqrt{\frac{1}{2}\int_{\Omega_v}r^2\,\mathrm{d}v}. \tag{3.27}$$

The following two lemmas present the properties of the operators $H^{x\pm}(r,s)$ and $H^{v\pm}(r,s)$ defined in (3.25). Lemma 3.4 states the skew-symmetric and semi-definite nature of these operators, while Lemma 3.5 provides an estimate for them. The proofs of these properties are straightforward, and are omitted here. For more detailed information, we refer to [61].

Lemma 3.4. For $r, s \in \mathbb{V}_h^k$, the following relations hold:

$$H^{x+}(r,s) = -H^{x,-}(s,r), \qquad H^{v+}(r,s) = -H^{v,-}(s,r)$$
$$H^{x-}(r,r) = -\frac{1}{2}[\![r]\!]_{(x)}^2, \qquad H^{v-}(r,r) = -\frac{1}{2}[\![r]\!]_{(v)}^2.$$

Lemma 3.5. For any $r, s \in \mathbb{V}_h^k$, there exist positive constants c_x, c_v independent of Δx and Δv such that

$$|H^{x\pm}(r,s)| \leqslant \frac{c_x}{\Delta x}\sqrt{\int_{\Omega_x} r^2 \,\mathrm{d}x}\sqrt{\int_{\Omega_x} s^2 \,\mathrm{d}x},$$
$$|H^{v\pm}(r,s)| \leqslant \frac{c_v}{\Delta v}\sqrt{\int_{\Omega_v} r^2 \,\mathrm{d}v}\sqrt{\int_{\Omega_v} s^2 \,\mathrm{d}v}.$$

Based on Lemma 3.3 and Lemma 3.5, we derive the following two corollaries.

Corollary 3.1. For $r \in \mathbb{V}_h^k$, we have

$$[\![r]\!]_{(v)} \leqslant \frac{c_1}{\sqrt{\Delta v}}\sqrt{\int_{\Omega_v} r^2 \,\mathrm{d}v}.$$

Corollary 3.2. For any $r, s \in \mathbb{V}_h^k$, we have

$$\int_{\Omega_v} |H^{x\pm}(r,s)| \,\mathrm{d}v \leqslant \frac{c_x}{\Delta x}\|r\|_2\|s\|_2,$$
$$\int_{\Omega_x} |H^{v\pm}(r,s)| \,\mathrm{d}x \leqslant \frac{c_v}{\Delta v}\|r\|_2\|s\|_2.$$

Theorem 3.3 (L^2 **stability**). Assume that there exist some positive constants M_u, M_E, M_T, such that

$$|u(x) - \overline{(u)}_{I_i}| \leqslant M_u \Delta x, \tag{3.28a}$$
$$|E(x) - \overline{(E)}_{I_i}| \leqslant M_E \Delta x, \tag{3.28b}$$
$$|T(x) - \overline{(T)}_{I_i}| \leqslant M_T \Delta x, \tag{3.28c}$$

for $x \in I_i$. Assume that the temperature $T > T_{\min} > 0$, and v, u, E, and J are bounded. Denote $\tau_x = \Delta t/\Delta x^2$, $\tau_v = \Delta t/\Delta v^2$. If $\tau_v \leqslant \frac{1}{2\nu c_v^2 T_{\max}} - \frac{M_T \Delta x}{4\nu c_v T_{\min} \Delta v}$, and τ_x is bounded, then the fully discrete explicit scheme (3.4) is L^2 stable for suitable small time step Δt, that is, there exists a constant C depending on $\nu, c_1, c_x, c_v, M_u, M_E, M_T, |v|_{\max}, |v-u|_{\max}, |E|_{\max}, T_{\min}, \tau_x, \tau_v, \Delta x/\Delta v$[R1], such that

$$\|f^n\|_2 \leqslant e^{Ct}\|f^0\|_2. \tag{3.29}$$

Proof. Let L_{E^n} denote the spatial discretization operator for (3.4a) and $L_{\frac{E^n+E^{n+1}}{2}}$ denote the spatial discretization operator for (3.4c). The fully discrete scheme (3.4) can be rewritten as

$$f^{n+\frac{1}{2}} = f^n + \frac{\Delta t}{2} L_{E^n}(f^n), \quad f^{n+1} = f^n + \Delta t L_{\frac{E^n+E^{n+1}}{2}}(f^{n+\frac{1}{2}}), \tag{3.30}$$

which, following the approach in [31], can be further rewritten as

$$f^{n+1} = \frac{1}{2}\big(I + \Delta t L_{\frac{E^n+E^{n+1}}{2}}\big)(I + \Delta t L_{E^n})(f^n) + \frac{1}{2}\big(I + \Delta t (L_{\frac{E^n+E^{n+1}}{2}} - L_{E^n})\big)(f^n), \tag{3.31}$$

where I denotes the identity operator. We establish the estimate of $\|f^{n+1}\|_2$ in the following three steps.

Step I: estimate of $\|(I + \Delta t L_{E^n})(f^n)\|_2$ and $\left\|(I + \Delta t L_{\frac{E^n+E^{n+1}}{2}})(f^n)\right\|_2$.

We first establish the estimate for $\|I + \Delta t L_{E^n}(f^n)\|_2$. For simplicity in presentation, we will omit the superscript n. We start by rewriting $L_E(f)$ as $L_E(f) = z_1 + z_2 + z_3 + q$, where $z_1, z_2, z_3, q \in \mathbb{V}_h^k$ satisfy

$$(z_1, \phi_1)_\Omega = \int_0^{+\infty} v H^{x-}(f, \phi_1)\, \mathrm{d}v + \int_{-\infty}^0 v H^{x+}(f, \phi_1)\, \mathrm{d}v, \tag{3.32a}$$

$$(z_2, \phi_2)_\Omega = \sum_{\substack{i \\ \overline{(E)}_{I_i} \geqslant 0}} \int_{I_i} E H^{v-}(f, \phi_2)\, \mathrm{d}x + \sum_{\substack{i \\ \overline{(E)}_{I_i} < 0}} \int_{I_i} E H^{v+}(f, \phi_2)\, \mathrm{d}x, \tag{3.32b}$$

$$\begin{aligned}(z_3, \phi_3)_\Omega = &-\nu \sum_{i,j} ((v-u)f, (\phi_3)_v)_{K_{ij}} + \nu \sum_{i,j} \Big\langle (v_{j+\frac{1}{2}} - u)\tilde{f}_{x,j+\frac{1}{2}}, \phi_3(x, v^-_{j+\frac{1}{2}}) \Big\rangle_{I_i} \\ &- \nu \sum_{i,j} \Big\langle (v_{j-\frac{1}{2}} - u)\tilde{f}_{x,j-\frac{1}{2}}, \phi_3(x, v^+_{j-\frac{1}{2}}) \Big\rangle_{I_i},\end{aligned} \tag{3.32c}$$

$$(q, \varphi)_\Omega = -\nu \int_{\Omega_x} H^{v+}(p, \varphi)\ \mathrm{d}x, \tag{3.32d}$$

for any test functions ϕ_1, ϕ_2, ϕ_3, and $\varphi \in \mathbb{V}_h^k$. Then we have

$$\begin{aligned}&\|(I + \Delta t L_E) f\|_2^2 \\ =&\|f\|_2^2 + 2\Delta t (z_1 + z_2 + z_3 + q, f)_\Omega + \Delta t^2 \|z_1 + z_2 + z_3 + q\|_2^2 \\ \leqslant&\|f\|_2^2 + 2\Delta t (z_1 + z_2 + z_3 + q, f)_\Omega + 4\Delta t^2 (\|z_1\|_2^2 + \|z_2\|_2^2 + \|z_3\|_2^2 + \|q\|_2^2).\end{aligned} \tag{3.33}$$

We estimate these terms one by one in the following. For the term $(z_1, f)_\Omega$, a simple use of Lemma 3.4 leads to

$$\begin{aligned}(z_1, f)_\Omega &= \int_0^{+\infty} v H^{x-}(f, f)\, \mathrm{d}v + \int_{-\infty}^0 v H^{x+}(f, f)\, \mathrm{d}v \\ &= -\frac{1}{2} \int_0^{+\infty} v \left[\!\left[f \right]\!\right]^2_{(x)}\ \mathrm{d}v + \frac{1}{2} \int_{-\infty}^0 v \left[\!\left[f \right]\!\right]^2_{(x)}\ \mathrm{d}v \\ &\leqslant 0.\end{aligned} \tag{3.34}$$

For the term $(z_2, f)_\Omega$, similar estimates can be conducted to obtain

$$\begin{aligned}
(z_2, f)_\Omega &= \sum_{\substack{i \\ \overline{(E)}_{I_i} \geqslant 0}} \int_{I_i} EH^{v-}(f, f)\,\mathrm{d}x + \sum_{\substack{i \\ \overline{(E)}_{I_i} < 0}} \int_{I_i} EH^{v+}(f, f)\ \mathrm{d}x \\
&= -\frac{1}{2} \sum_{\substack{i \\ \overline{(E)}_{I_i} \geqslant 0}} \int_{I_i} E \left[\!\left[f\right]\!\right]^2_{(v)}\ \mathrm{d}x + \frac{1}{2} \sum_{\substack{i \\ \overline{(E)}_{I_i} < 0}} \int_{I_i} E \left[\!\left[f\right]\!\right]^2_{(v)}\ \mathrm{d}x \\
&= -\frac{1}{2} \sum_{\substack{i \\ \overline{(E)}_{I_i} \geqslant 0}} \int_{I_i} (E - \overline{(E)}_{I_i}) \left[\!\left[f\right]\!\right]^2_{(v)}\ \mathrm{d}x - \frac{1}{2} \sum_{\substack{i \\ \overline{(E)}_{I_i} \geqslant 0}} \int_{I_i} \overline{(E)}_{I_i} \left[\!\left[f\right]\!\right]^2_{(v)}\ \mathrm{d}x \\
&\quad + \frac{1}{2} \sum_{\substack{i \\ \overline{(E)}_{I_i} < 0}} \int_{I_i} (E - \overline{(E)}_{I_i}) \left[\!\left[f\right]\!\right]^2_{(v)}\ \mathrm{d}x + \frac{1}{2} \sum_{\substack{i \\ \overline{(E)}_{I_i} < 0}} \int_{I_i} \overline{(E)}_{I_i} \left[\!\left[f\right]\!\right]^2_{(v)}\ \mathrm{d}x \\
&\leqslant -\frac{1}{2} \sum_{\substack{i \\ \overline{(E)}_{I_i} \geqslant 0}} \int_{I_i} (E - \overline{(E)}_{I_i}) \left[\!\left[f\right]\!\right]^2_{(v)}\ \mathrm{d}x + \frac{1}{2} \sum_{\substack{i \\ \overline{(E)}_{I_i} < 0}} \int_{I_i} (E - \overline{(E)}_{I_i}) \left[\!\left[f\right]\!\right]^2_{(v)}\ \mathrm{d}x \\
&\leqslant \frac{1}{2} \sum_i \int_{I_i} \left|E - \overline{(E)}_{I_i}\right| \left[\!\left[f\right]\!\right]^2_{(v)}\ \mathrm{d}x,
\end{aligned}$$

which, together with the assumption (3.28b) and Corollary 3.1, yields

$$(z_2, f)_\Omega \leqslant \frac{M_E \Delta x}{2} \sum_i \int_{I_i} \left(\frac{c_1}{\sqrt{\Delta v}} \sqrt{\int_{\Omega_v} f^2\ \mathrm{d}v} \right)^2 \mathrm{d}x = \frac{c_1^2 M_E \Delta x}{2\Delta v} \|f\|_2^2. \tag{3.35}$$

For the term $(z_3, f)_\Omega$, it follows from integration by parts that

$$\begin{aligned}
(z_3, f)_\Omega &= -\nu \sum_{i,j} ((v-u)f, f_v)_{K_{ij}} + \nu \sum_{i,j} \left\langle (v_{j+\frac{1}{2}} - u) \tilde{f}_{x,j+\frac{1}{2}}, f(x, v^-_{j+\frac{1}{2}}) \right\rangle_{I_i} \\
&\quad - \nu \sum_{i,j} \left\langle (v_{j-\frac{1}{2}} - u) \tilde{f}_{x,j-\frac{1}{2}}, f(x, v^+_{j-\frac{1}{2}}) \right\rangle_{I_i} \\
&= \frac{\nu}{2} \|f\|_2^2 + \frac{\nu}{2} \sum_{i,j} \int_{I_i} \left(-(v_{j+\frac{1}{2}} - u) f^2(x, v^-_{j+\frac{1}{2}}) + (v_{j-\frac{1}{2}} - u) f^2(x, v^+_{j-\frac{1}{2}}) \right) \mathrm{d}x \\
&\quad + \nu \sum_{i,j} \left(\left\langle (v_{j+\frac{1}{2}} - u) \tilde{f}_{x,j+\frac{1}{2}}, f(x, v^-_{j+\frac{1}{2}}) \right\rangle_{I_i} - \left\langle (v_{j-\frac{1}{2}} - u) \tilde{f}_{x,j-\frac{1}{2}}, f(x, v^+_{j-\frac{1}{2}}) \right\rangle_{I_i} \right) \\
&= \frac{\nu}{2} \|f\|_2^2 + \frac{\nu}{2} \sum_{\substack{i \\ v_{j+\frac{1}{2}} \leqslant \overline{(u)}_{I_i}}} \int_{I_i} (v_{j+\frac{1}{2}} - u) \left[\!\left[f\right]\!\right]^2_{(v)}\ \mathrm{d}x - \frac{\nu}{2} \sum_{\substack{i \\ v_{j+\frac{1}{2}} > \overline{(u)}_{I_i}}} \int_{I_i} (v_{j+\frac{1}{2}} - u) \left[\!\left[f\right]\!\right]^2_{(v)} \mathrm{d}x,
\end{aligned}$$

which follows the similar line as the estimate of $(z_2, f)_\Omega$, yielding

$$(z_3, f)_\Omega \leqslant \frac{\nu}{2} \|f\|_2^2 + \frac{\nu}{2} \sum_i \int_{I_i} |u - \overline{(u)}_{I_i}| \left[\!\left[f\right]\!\right]^2_{(v)}\ \mathrm{d}x \leqslant \frac{\nu}{2} \|f\|_2^2 + \frac{\nu c_1^2 M_u \Delta x}{2\Delta v} \|f\|_2^2. \tag{3.36}$$

For the term $\|z_1\|_2^2$, by taking $\phi_1 = z_1$ in (3.32a) and Corollary 3.2, we have

$$\|z_1\|_2^2 = \int_0^{+\infty} vH^{x-}(f, z_1)\,\mathrm{d}v + \int_{-\infty}^{0} vH^{x+}(f, z_1)\,\mathrm{d}v \leqslant \frac{c_x}{\Delta x}|v|_{\max}\|f\|_2\|z_1\|_2,$$

which yields

$$\|z_1\|_2^2 \leqslant \frac{c_x^2}{\Delta x^2}|v|_{\max}^2\|f\|_2^2. \tag{3.37}$$

For the terms $\|z_2\|_2^2$ and $\|q\|_2^2$, similar estimates can be conducted to obtain

$$\|z_2\|_2^2 \leqslant \frac{c_v^2}{\Delta v^2}|E|_{\max}^2\|f\|_2^2, \tag{3.38}$$

$$\|q\|_2^2 \leqslant \frac{\nu^2 c_v^2}{\Delta v^2}\|p\|_2^2. \tag{3.39}$$

For the term $\|z_3\|$, by taking $\phi_3 = z_3$ in (3.32c), we rewrite it as

$$\begin{aligned}
\|z_3\|_2^2 &= -\nu\sum_{i,j}\left((v-u)f, (z_3)_v\right)_{K_{ij}} + \nu\sum_{i,j}\left\langle (v_{j+\frac{1}{2}}-u)\tilde{f}_{x,j+\frac{1}{2}}, z_3(x, v_{j+\frac{1}{2}}^-)\right\rangle_{I_i} \\
&\quad - \nu\sum_{i,j}\left\langle (v_{j-\frac{1}{2}}-u)\tilde{f}_{x,j-\frac{1}{2}}, z_3(x, v_{j-\frac{1}{2}}^+)\right\rangle_{I_i} \\
&= -\nu\sum_{i,j}\left((v-u)f, (z_3)_v\right)_{K_{ij}} + \nu\sum_{i,j}\left\langle (v_{j+\frac{1}{2}}-u)\tilde{f}_{x,j+\frac{1}{2}}, z_3(x, v_{j+\frac{1}{2}}^-)\right\rangle_{I_i} \\
&\quad - \nu\sum_{i,j}\left\langle (v_{j+\frac{1}{2}}-u)\tilde{f}_{x,j+\frac{1}{2}}, z_3(x, v_{j+\frac{1}{2}}^+)\right\rangle_{I_i} \\
&= -\nu\sum_{i,j}\left((v-u)f, (z_3)_v\right)_{K_{ij}} + \nu\sum_{i,j}\left\langle (v_{j+\frac{1}{2}}-u)\tilde{f}_{x,j+\frac{1}{2}}, (z_3(x, v_{j+\frac{1}{2}}^-) - z_3(x, v_{j+\frac{1}{2}}^+))\right\rangle_{I_i},
\end{aligned}$$

which, together with the Cauchy-Schwarz inequality and Lemma 3.3, yields

$$\begin{aligned}
\|z_3\|_2^2 &\leqslant \nu|v-u|_{\max}\|f\|_2\|(z_3)_v\|_2 + \nu|v-u|_{\max}\int_{\Omega_x}\sqrt{\sum_j (f^2(x, v_{j+\frac{1}{2}}^+) + f^2(x, v_{j+\frac{1}{2}}^-))}\,[\![z_3]\!]_{(v)}\,\mathrm{d}x \\
&\leqslant \frac{\nu|v-u|_{\max}c_1(1+c_1)}{\sqrt{2}\Delta v}\|f\|_2\|z_3\|_2,
\end{aligned}$$

which further leads to

$$\|z_3\|_2^2 \leqslant \frac{\nu^2 c_1^2(1+c_1)^2}{2(\Delta v)^2}|v-u|_{\max}^2\|f\|_2^2. \tag{3.40}$$

For the term $(q, f)_\Omega$, it follows from Lemma 3.4 that

$$\sum_j (q, f)_{K_{ij}} = -\nu\int_{I_i} H^{v+}(p, f)\,\mathrm{d}x = \nu\int_{I_i} H^{v-}(f, p)\,\mathrm{d}x. \tag{3.41}$$

On the other hand, it follows from (3.4d) and the definition in (3.25b) that

$$\sum_j (p,p)_{K_{ij}} = -\int_{I_i} TH^{v-}(f,p)\,\mathrm{d}x. \tag{3.42}$$

Then, by rewriting $(q,f)_\Omega$ based on (3.41) and (3.42) and applying the assumption (3.28c) and Corollary 3.2, we have

$$\begin{aligned}
(q,f)_\Omega &= \sum_i \left(\frac{\nu}{\overline{(\overline{T})}_{I_i}} \int_{I_i} TH^{v-}(f,p)\,\mathrm{d}x + \frac{\nu}{\overline{(\overline{T})}_{I_i}} \int_{I_i} (\overline{(\overline{T})}_{I_i} - T) H^{v-}(f,p)\,\mathrm{d}x \right) \\
&\leqslant -\frac{\nu}{T_{\max}}(p,p)_\Omega + \nu \max_i \frac{1}{\overline{(\overline{T})}_{I_i}} \int_{\Omega_x} |T - \overline{(\overline{T})}_i| |H^{v-}(f,p)|\,\mathrm{d}x \\
&\leqslant -\frac{\nu}{T_{\max}}(p,p)_\Omega + \frac{\nu M_T c_v \Delta x}{T_{\min}\Delta v}\|f\|_2\|p\|_2 \\
&\leqslant \left(-\frac{\nu}{T_{\max}} + \frac{\nu M_T c_v \Delta x}{2T_{\min}\Delta v} \right) \|p\|_2^2 + \frac{\nu M_T c_v \Delta x}{2T_{\min}\Delta v}\|f\|_2^2,
\end{aligned} \tag{3.43}$$

which, together with (3.39), for $\tau_v \leqslant \frac{1}{2\nu c_v^2 T_{\max}} - \frac{M_T \Delta x}{4c_v T_{\min}\Delta v}$, yields

$$\begin{aligned}
\Delta t(q,f)_\Omega + 2\Delta^2(q,q)_\Omega &\leqslant \nu\Delta t(-\frac{1}{T_{\max}} + \frac{\nu M_T c_v \Delta x}{2T_{\min}\Delta v} + 2\nu c_v^2 \tau_v) + \Delta t \frac{\nu M_T c_v \Delta x}{2T_{\min}\Delta v}\|f\|_2^2 \\
&\leqslant \Delta t \frac{\nu M_T c_v \Delta x}{2T_{\min}\Delta v}\|f\|_2^2.
\end{aligned} \tag{3.44}$$

By substituting (3.34), (3.35), (3.36), (3.37), (3.38), (3.40), and (3.44) into (3.33), and recovering the superscript n, we obtain

$$\|(I + \Delta t L_{E^n})(f^n)\|_2^2 \leqslant (1 + C_0\Delta t)\,\|f^n\|_2^2, \tag{3.45}$$

with

$$C_0 = 4c_x^2|v|_{\max}^2\tau_x + 4c_v^2|E|_{\max}^2\tau_v + \nu + 2\nu^2 c_1^2(1+c_1)^2\tau_v|v-u|_{\max}^2 + (c_1^2 M_E + \nu c_1^2 M_u + M_T c_v T_{\min})\frac{\Delta x}{\Delta v}.$$

The estimate of $\|(I + \Delta t L_{\frac{E^n+E^{n+1}}{2}})(f^n)\|_2$ follows a similar approach as the estimate of $\|(I + \Delta t L_{E^n})(f^n)\|_2$. The difference lies in the terms associated to z_2 defined in (3.32b), i.e., $(z_2,f)_\Omega$ and $\|z_2\|_2^2$. It can be verified that, with the assumption (3.28b) and E is bounded, there hold

$$\left| \frac{E^n + E^{n+1}}{2} - \frac{\overline{(E^n + E^{n+1})}_{I_i}}{2} \right| \leqslant \left| \frac{E^n - \overline{(E^n)}_{I_i}}{2} \right| + \left| \frac{E^{n+1} - \overline{(E^{n+1})}_{I_i}}{2} \right| \leqslant M_E \Delta x, \tag{3.46a}$$

$$\left| \frac{E^n + E^{n+1}}{2} \right|_{\max}^2 \leqslant \frac{|E^n|_{\max}^2 + |E^{n+1}|_{\max}^2}{2} \leqslant |E|_{\max}^2, \tag{3.46b}$$

which leads to the same estimates in (3.35) and (3.38) when changing E^n to $\frac{E^n+E^{n+1}}{2}$, and further yields

$$\left\|(I+\Delta t L_{\frac{E^n+E^{n+1}}{2}})(f^n)\right\|_2^2 \leqslant (1+C_0\Delta t)\left\|f^n\right\|_2^2. \tag{3.47}$$

Step II: estimate of $\left\|\left(L_{\frac{E^n+E^{n+1}}{2}}-L_{E^n}\right)(f^n)\right\|_2$.

As mentioned in Step I, the difference between the operators L_{E^n} and $L_{\frac{E^n+E^{n+1}}{2}}-L_{E^n}$ lies in the terms associated to z_2 defined in (3.32b). To highlight this difference, we introduce a modified notation for z_2, denoting it as $(z_2)_E$. Then, we have

$$\left(L_{\frac{E^n+E^{n+1}}{2}}-L_{E^n}\right)(f^n) = (z_2)_{\frac{E^n+E^{n+1}}{2}} - (z_2)_{E^n}.$$

To simplify the presentation, we introduce the following two index sets. Denote I_A as $I_A=\left\{i \mid \overline{\left(\frac{E^n+E^{n+1}}{2}\right)}_{I_i} \geqslant 0\right\}$, I_B as $I_B=\{i \mid \overline{(E^n)}_{I_i} \geqslant 0\}$, and their complement sets as $I_A^{\complement}$ and $I_B^{\complement}$, respectively. It follows from (3.4b) that $\frac{E^n+E^{n+1}}{2}=E^n-\frac{\Delta t}{2}J^{n+\frac{1}{2}}$, which yields

$$I_A\cap I_B^{\complement}=\left\{i \mid \frac{\Delta t}{2}\overline{\left(J^{n+\frac{1}{2}}\right)}_{I_i} \leqslant \overline{(E^n)}_{I_i}<0\right\}=\left\{i \mid 0\leqslant \overline{\left(\frac{E^n+E^{n+1}}{2}\right)}_{I_i}<-\frac{\Delta t}{2}\overline{\left(J^{n+\frac{1}{2}}\right)}_{I_i}\right\},$$

$$I_A^{\complement}\cap B=\left\{i \mid \frac{\Delta t}{2}\overline{(J^{n+\frac{1}{2}})}_{I_i} > \overline{(E^n)}_{I_i}\geqslant 0\right\}=\left\{i \mid 0> \overline{\left(\frac{E^n+E^{n+1}}{2}\right)}_{I_i}\geqslant -\frac{\Delta t}{2}\overline{\left(J^{n+\frac{1}{2}}\right)}_{I_i}\right\}.$$

Therefore, for any $x\in I_i,\ i\in (I_A\cap I_B^{\complement})\cup(I_A^{\complement}\cap I_B)$, we have

$$|\overline{(E^n)}_{I_i}|\leqslant\frac{|J|_{\max}\Delta t}{2},\qquad \left|\frac{\overline{(E^n)}_{I_i}+\overline{(E^{n+1})}_{I_i}}{2}\right|\leqslant\frac{|J|_{\max}\Delta t}{2},$$

which, combining with the assumption (3.28b) and (3.46a), leads to

$$|E^n|\leqslant\frac{|J|_{\max}\Delta t}{2}+M_E\Delta x,\quad \left|\frac{E^n+E^{n+1}}{2}\right|\leqslant\frac{|J|_{\max}\Delta t}{2}+M_E\Delta x.$$

With these notations and relations, following (3.4b), the definition of z_2 in (3.32b) and

Lemma 3.5, for any function $\phi \in \mathbb{V}_h^k$, we have

$$
\begin{aligned}
&\left(\left(L_{\frac{E^n+E^{n+1}}{2}} - L_{E^n}\right)(f^n), \phi\right)_\Omega = \left((z_2)_{\frac{E^n+E^{n+1}}{2}} - (z_2)_{E^n}, \phi\right)_\Omega \\
=& \sum_{i\in I_A} \int_{I_i} \frac{E^n+E^{n+1}}{2} H^{v-}(f^n,\phi)\,\mathrm{d}x + \sum_{i\in I_A^\complement} \int_{I_i} \frac{E^n+E^{n+1}}{2} H^{v+}(f^n,\phi)\,\mathrm{d}x \\
&- \sum_{i\in I_B} \int_{I_i} E^n H^{v-}(f^n,\phi)\,\mathrm{d}x - \sum_{i\in (I_B^\complement)} \int_{I_i} E^n H^{v+}(f^n,\phi)\,\mathrm{d}x \\
=& \sum_{i\in (I_A\cap I_B)} \int_{I_i} \left(\frac{E^n+E^{n+1}}{2} - E^n\right) H^{v-}(f^n,\phi)\,\mathrm{d}x + \sum_{i\in (I_A^\complement\cap I_B^\complement)} \left(\frac{E^n+E^{n+1}}{2} - E^n\right) H^{v+}(f^n,\phi)\,\mathrm{d}x \\
&+ \sum_{i\in (I_A\cap I_B^\complement)} \int_{I_i} \left(\frac{E^n+E^{n+1}}{2} H^{v-}(f^n,\phi) - E^n H^{v+}(f^n,\phi)\right)\mathrm{d}x \\
&+ \sum_{i\in (I_A^\complement\cap I_B)} \int_{I_i} \left(\frac{E^n+E^{n+1}}{2} H^{v+}(f^n,\phi) - E^n H^{v-}(f^n,\phi)\right)\mathrm{d}x \\
\leqslant& \frac{|J|_{\max}\Delta t}{2} \sum_{i\in (I_A\cap I_B)} \int_{I_i} |H^{v-}(f^n,\phi)|\,\mathrm{d}x + \frac{|J|_{\max}\Delta t}{2} \sum_{i\in (I_A^\complement\cap I_B^\complement)} \int_{I_i} |H^{v+}(f^n,\phi)|\,\mathrm{d}x \\
&+ \left(\frac{|J|_{\max}\Delta t}{2} + M_E\Delta x\right) \sum_{i\in (I_A\cap I_B^\complement)\cup (I_A^\complement\cap I_B)} \int_{I_i} |H^{v-}(f^n,\phi)| + |H^{v+}(f^n,\phi)|\,\mathrm{d}x \\
\leqslant& \frac{c_v}{\Delta v}(|J|_{\max}\Delta t + 2M_E\Delta x) \int_{\Omega_x} \sqrt{\int_{\Omega_v} (f^n)^2\,\mathrm{d}v} \sqrt{\int_{\Omega_v} (\phi)^2\,\mathrm{d}v}\,\mathrm{d}x \\
\leqslant& \left(\frac{c_v|J|_{\max}\Delta t}{\Delta v} + \frac{2c_v M_E\Delta x}{\Delta v}\right)\|f^n\|_2\|\phi\|_2,
\end{aligned}
$$

By taking $\phi = \left(L_{\frac{E^n+E^{n+1}}{2}} - L_{E^n}\right)(f^n)$, we obtain

$$
\left\|\left(L_{\frac{E^n+E^{n+1}}{2}} - L_{E^n}\right)(f^n)\right\|_2 \leqslant \left(\frac{c_v|J|_{\max}\Delta t}{\Delta v} + \frac{2c_v M_E\Delta x}{\Delta v}\right)\|f^n\|_2. \tag{3.48}
$$

Step III: final estimate of $\|f^{n+1}\|_2$.

By applying the triangle inequality to (3.31) and combining with the estimates in (3.45), (3.47), and (3.48), we have

$$
\begin{aligned}
\|f^{n+1}\|_2 &\leqslant \frac{1}{2}\|(I+\Delta t L_{\frac{E^n+E^{n+1}}{2}})(I+\Delta t L_{E^n})f^n\|_2 + \frac{1}{2}\|f^n\|_2 + \frac{1}{2}\Delta t\|(L_{\frac{E^n+E^{n+1}}{2}} - L_{E^n})f^n\|_2 \\
&\leqslant \frac{1}{2}\sqrt{1+C_0\Delta t}\|(I+\Delta t L_{E^n})f^n\|_2 + \frac{1}{2}\|f^n\|_2 + \frac{1}{2}\Delta t\left(\frac{c_v|J|_{\max}\Delta t}{\Delta v} + \frac{2c_v M_E\Delta x}{\Delta v}\right)\|f^n\|_2 \\
&\leqslant \left(1 + \left(\frac{C_0}{2} + \frac{c_v M_E\Delta x}{\Delta v} + \frac{c_v|J|_{\max}\Delta t}{2\Delta v}\right)\Delta t\right)\|f^n\|_2.
\end{aligned}
$$

By choosing small enough Δt such that $\Delta t \leqslant \frac{2\Delta v}{c_v |J|_{\max}}$, we have

$$\|f^n\|_2 \leqslant e^{(\frac{C_0}{2} + \frac{c_v M_E \Delta x}{\Delta v} + 1)t} \|f^0\|_2. \tag{3.49}$$

We complete the proof by setting $C = \frac{C_0}{2} + \frac{c_v M_E \Delta x}{\Delta v} + 1$. □

4 Numerical results

In this section, we present numerical examples to demonstrate the accuracy and performance of the proposed schemes.

4.1 Accuracy tests

In this subsection, we use two examples to test the orders of accuracy of the proposed schemes.

Example 4.1 (**Relaxation to Maxwellian**). In this example, we consider a simplified ~~example~~[R2] case[R2] only involving the DFP operator, given by

$$f_t = Q(f) = T f_{vv} + [(v-u)f]_v, \quad v \in [-16.5, 15.5], \tag{4.1}$$

with the initial condition

$$f(0,v) = \frac{1}{\sqrt{2\pi}} \left(\frac{1}{2} \exp\left(-\frac{(v-1)^2}{2} \right) + \frac{1}{2} \exp\left(-\frac{(v+2)^2}{2} \right) \right), \tag{4.2}$$

which is inspired by a mixture of two Gaussian distributions. Here the average velocity $u = -0.5$, the ~~thermal~~[R2] temperature $T = 3.25$, and the density $\rho = 1$. As the system evolves, these three quantities do not change, and the system would eventually approach a steady state described by the Maxwellian function:

$$f(\infty, v) = \frac{\rho}{\sqrt{2\pi T}} \exp\left(-\frac{(v-u)^2}{2T} \right) = \frac{1}{\sqrt{6.5\pi}} \exp\left(-\frac{(v+0.5)^2}{6.5} \right). \tag{4.3}$$

We perform numerical simulations using the LDG method with the explicit time integrator (2.1) up to $t_{end} = 2$. To match the accuracy of the temporal and spatial discretizations, we adjust the time step Δt as $\Delta t \sim (\Delta v)^{\frac{3}{2}}$ for P^2 polynomials and $\Delta t \sim (\Delta v)^2$ for P^3 polynomials. Table 4.1 lists the L^1 and L^∞ errors and orders between the numerical solution and the steady state. It can be observed that for both polynomial spaces, the scheme can achieve optimal $(k+1)$-th order of accuracy.

Table 4.1: L^1, $L^{2\text{R2}}$ and L^∞ errors and orders for Example 4.1 using the explicit scheme (2.1).

	P^2					
N_v	L^1 error	Order	L^2 error$^{\text{R2}}$	Order$^{\text{R2}}$	L^∞ error	Order
30	1.23E-03		5.22E-04$^{\text{R2}}$		7.04E-04	
40	5.17E-04	3.02	2.24E-04$^{\text{R2}}$	2.95$^{\text{R2}}$	3.41E-04	2.69
50	2.64E-04	3.01	1.15E-04$^{\text{R2}}$	2.96$^{\text{R2}}$	1.66E-04	3.23
75	7.77E-05	3.02	3.45E-05$^{\text{R2}}$	2.98$^{\text{R2}}$	5.27E-05	2.83
100	3.30E-05	2.98	1.46E-05$^{\text{R2}}$	2.99$^{\text{R2}}$	2.21E-05	3.03
	P^3					
N_v	L^1 error	Order	L^2 error$^{\text{R2}}$	Order$^{\text{R2}}$	L^∞ error	Order
30	8.13E-05		3.59E-05$^{\text{R2}}$		5.07E-05	
40	2.53E-05	4.06	1.15E-05$^{\text{R2}}$	3.96$^{\text{R2}}$	1.75E-05	3.70
50	1.06E-05	3.89	4.75E-06$^{\text{R2}}$	3.97$^{\text{R2}}$	7.45E-06	3.82
75	2.08E-06	4.02	9.44E-07$^{\text{R2}}$	3.98$^{\text{R2}}$	1.57E-06	3.84
100	6.64E-07	3.96	3.00E-07$^{\text{R2}}$	3.99$^{\text{R2}}$	4.97E-07	4.02

Example 4.2 (Landau damping). In this example, we consider the VA-DFP equation (3.1) with $\nu = 0.01$. The initial conditions is given by

$$f_0(x,v) = f_M(v)(1 + A\cos(\kappa x)), \quad x \in [0, L], \quad v \in [-V_c, V_c], \tag{4.4}$$

with $A = 0.5, \kappa = 0.5, L = 4\pi, V_c = 12$, and $f_M = \frac{1}{\sqrt{2\pi}} e^{-v^2/2}$.

We simulate this example up to $t_{end} = 1$ and compute the error between the numerical solution with $N_x \times N_v$ cells and with $(1.5N_x) \times (1.5N_v)$ cells to test the order of accuracy. The DG method adopt P^2 polynomials. The time step is again adjusted as $\Delta t \sim (\Delta v)^{\frac{3}{2}}$ to match the accuracy of the temporal and spatial discretizations. Specifically, we set $\Delta t = 0.887622(\Delta x)^3$ for the explicit scheme and $\Delta t = 0.988524(\Delta x)^3$ for the IMEX scheme. Table 4.2 lists the L^1 and L^∞ errors and orders of accuracy for the explicit scheme and the IMEX scheme. We observe that both schemes achieve optimal third-order accuracy for the L^1 and L^2 errors$^{\text{R2}}$.

4.2 Benchmark examples

In this section, we demonstrate the conservation properties and performance of the explicit scheme (2.1) and the IMEX scheme (2.2) with P^2 DG polynomial spaces on a 50×100 meshes.

Table 4.2: L^1, $L^{2\text{R2}}$ and L^∞ errors and orders of accuracy for Example 4.2.

	Explicit					
$N_x \times N_v$	L^1 error	Order	L^2 error$^{\text{R2}}$	Order$^{\text{R2}}$	L^∞ error	Order
24×48	1.00E-00		1.93E-01$^{\text{R2}}$		1.51E-01	
36×72	3.19E-01	2.82	6.03E-02$^{\text{R2}}$	2.86$^{\text{R2}}$	4.95E-02	2.75
54×108	9.68E-02	2.94	1.83E-02$^{\text{R2}}$	2.94$^{\text{R2}}$	1.69E-02	2.65
81×162	3.06E-02	2.84	5.80E-03$^{\text{R2}}$	2.83$^{\text{R2}}$	6.60E-03	2.33
	IMEX					
$N_x \times N_v$	L^1 error	Order	L^2 error$^{\text{R2}}$	Order$^{\text{R2}}$	L^∞ error	Order
24×48	1.02E-00		1.99E-01$^{\text{R2}}$		1.55E-01	
36×72	3.24E-01	2.84	6.22E-02$^{\text{R2}}$	2.87$^{\text{R2}}$	5.15E-02	2.72
54×108	9.76E-02	2.96	1.87E-02$^{\text{R2}}$	2.96$^{\text{R2}}$	1.76E-02	2.65
81×162	3.00E-02	2.91	5.60E-03$^{\text{R2}}$	2.97$^{\text{R2}}$	4.80E-03	3.21

We also investigate different settings of ν. For small ν, the time step size for the explicit scheme (2.1) and the IMEX scheme (2.2) are almost the same. However, for $\nu = 1$, the IMEX scheme can utilize a time step of $\Delta t = 2.03 \times 10^{-3}$, which is much larger than the time step size of $\Delta t = 2.62 \times 10^{-4}$ for the explicit scheme. This results in considerable computational time savings. We list an empirical time step comparison in Table 4.3:$^{\text{R2}}$

Table 4.3: Time step comparison of the explicit scheme and the IMEX scheme for different ν.$^{\text{R2}}$

ν	0	0.1	0.5	1
Explicit	1.25E-03	7.86E-04	4.10E-04	2.57E-04
IMEX	2.03E-03	2.03E-03	2.03E-03	2.03E-03

We consider three benchmark examples of the VA-DFP system (3.1) with the following initial conditions:

Example 4.3 (**Landau damping**). In this example, ~~the initial condition is given by~~$^{\text{R2}}$

$$f_0(x,v) = f_M(v)(1 + A\cos(\kappa x)), \quad x \in [0, L], \quad v \in [-V_c, V_c],^{\text{R2}} \tag{4.5}$$

~~with $\kappa = 0.5, L = 4\pi, V_c = 12, f_M = \frac{1}{\sqrt{2\pi}} e^{-v^2/2}$. We~~$^{\text{R2}}$ we$^{\text{R2}}$ consider two additional$^{\text{R2}}$ cases of A: $A = 0.01$ *(weak Landau damping)* and $A = 0.5$ *(strong Landau damping)*. The governing equation and other initial condition remain consistent with those delineated in Example 4.2.$^{\text{R2}}$

Example 4.4 (**Two-stream instability**). In this example, the initial condition is given by

$$f_0(x,v) = f_{TS}(v)(1 + A\cos(\kappa x)), \quad x \in [0, L], \quad v \in [-V_c, V_c], \tag{4.6}$$

with $A = 0.05, \kappa = 0.5, L = 4\pi, V_c = 16, f_{TS} = \frac{1}{\sqrt{2\pi}} v^2 e^{-v^2/2}$.

Example 4.5 (**Bump-on-tail instability**). In this example, the initial condition is given by

$$f_0(x,v) = f_{BT}(v)(1 + A\cos(\kappa x)), \quad x \in [0, L], \quad v \in [-V_c, V_c], \tag{4.7}$$

with $A = 0.04, \kappa = 0.3, L = 20\pi/3, V_c = 16$, and

$$f_{BT}(v) = n_p \exp(-v^2/2) + n_b \exp(-\frac{|v-u|^2}{2v_t^2}), \tag{4.8}$$

whose parameters are

$$n_p = \frac{9}{10\sqrt{2\pi}}, \quad n_b = \frac{2}{10\sqrt{2\pi}}, \quad u = 4.5, \quad v_t = 0.5. \tag{4.9}$$

We first verify the conservation properties of the proposed schemes. Figures 4.1 and 4.2 plot the relative errors of the total particle number and total energy for the weak Landau damping and strong Landau damping of Example 4.3 with different values of ν. It can be observed that the absolute values of all errors with both schemes stay small, below 10^{-11} for the total particle number, 10^{-11} for the total energy of the weak Landau damping, and 10^{-8} for the total energy of strong Landau damping. Figures 4.3 and 4.4 plot the relative errors of the total particle number and total energy for two-stream instability of Example 4.4 and bump-on-tail instability of Example 4.5 with different values of ν. Again the absolute values of the observed relative errors remain low, below 10^{-11} for the total particle numbers and ~~10^{-10}~~R2 10^{-9} for the total energy. For all four examples, the conservation with the explicit scheme is slightly better than the IMEX scheme.

We further collect numerical data to benchmark our schemes. Both the fully explicit scheme and the fully IMEX scheme obtain equally good results. Thus, we we only show the results obtained with the explicit scheme to save space. Figure 4.5 plots the electric energy, the enstrophy and the entropy, which are defined as

$$E_p = \int_{\Omega_x} \frac{E^2}{2}\,\mathrm{d}x, \quad E_s = \int_{\Omega_x}\int_{\Omega_v} f^2\,\mathrm{d}x\,\mathrm{d}v, \quad S = -\int_{\Omega_x}\int_{\Omega_v} f\log f\,\mathrm{d}x\,\mathrm{d}v, \tag{4.10}$$

for both weak and strong Landau damping in Example 4.3 with various ν values. It can be observed that for weak Landau damping with $\nu = 0$, the electric field damps exponentially over time as expected from linearized analysis. We also observe that the electric field fails to damp after a long time, known as the recurrence phenomenon of numerical simulations. This

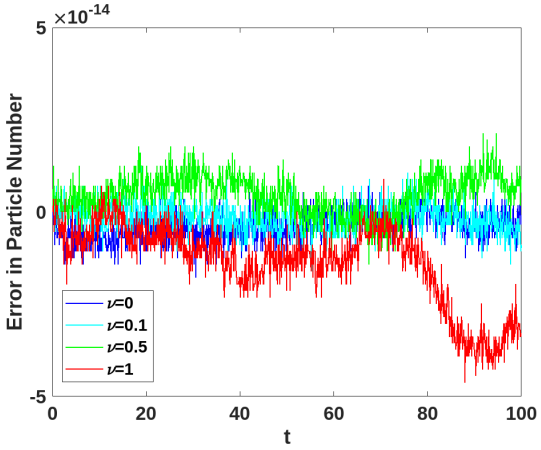

(a) Total particle number. Explicit.

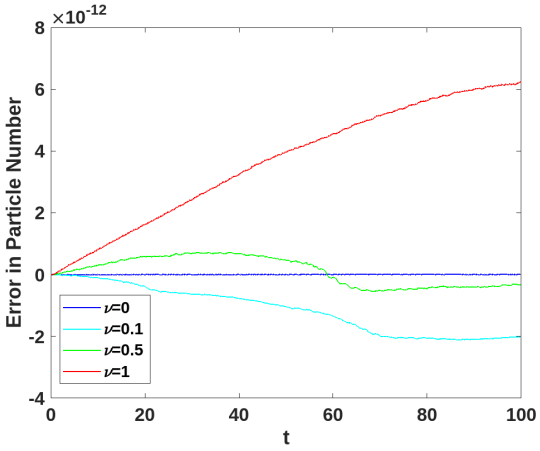

(b) Total particle number. IMEX.

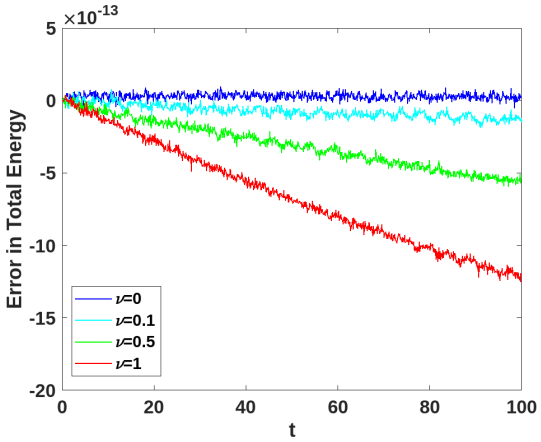

(c) Total energy. Explicit.

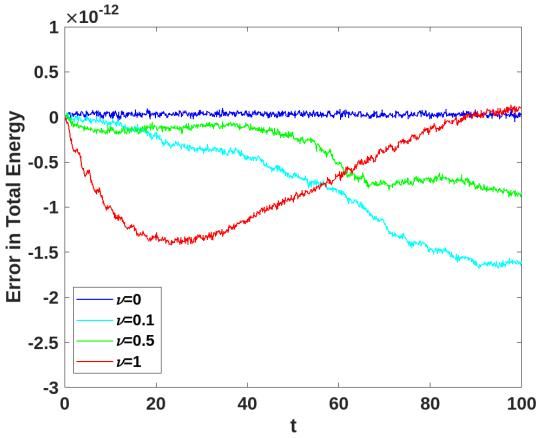

(d) Total energy. IMEX.

Figure 4.1: Weak Landau damping ($A = 0.01$) in Example 4.3. Evolution of the relative error in total particle number (top) and total energy (bottom) by the explicit scheme (left) and the IMEX scheme (right). 50×100 mesh.

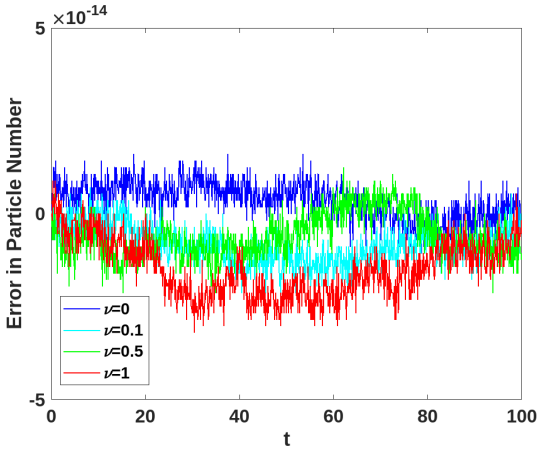

(a) Total particle number. Explicit.

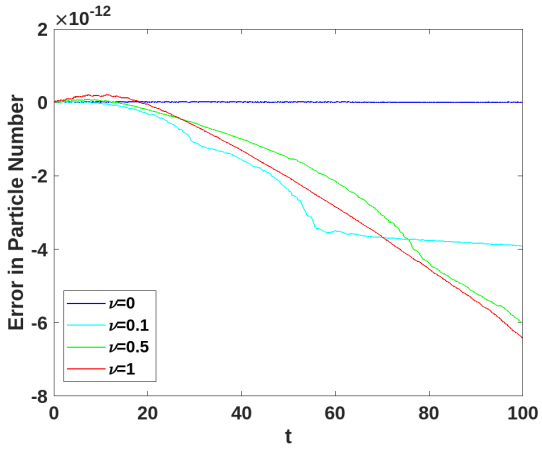

(b) Total particle number. IMEX.

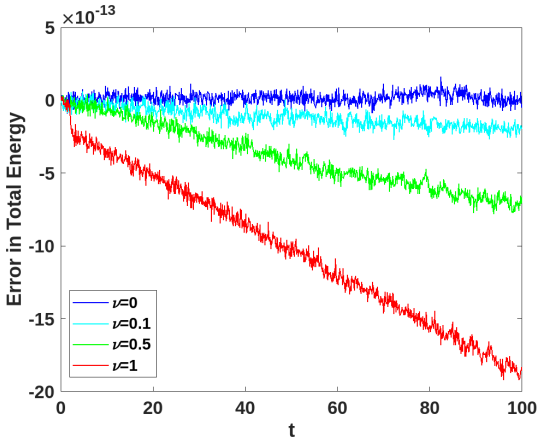

(c) Total energy. Explicit.

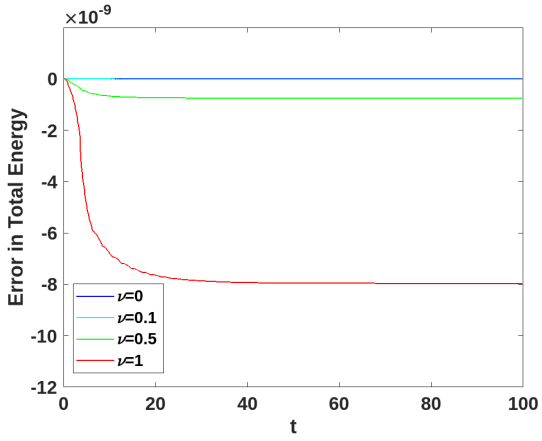

(d) Total energy. IMEX.

Figure 4.2: Strong Landau damping ($A = 0.5$) in Example 4.3. Evolution of the relative error in total particle number (top) and total energy (bottom) by the explicit scheme (left) and the IMEX scheme (right). 50×100 mesh.

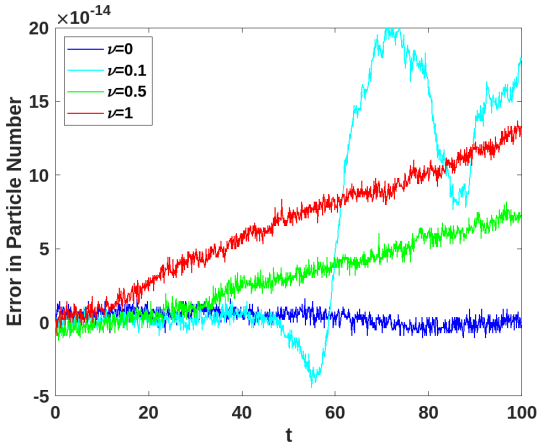

(a) Total particle number. Explicit.

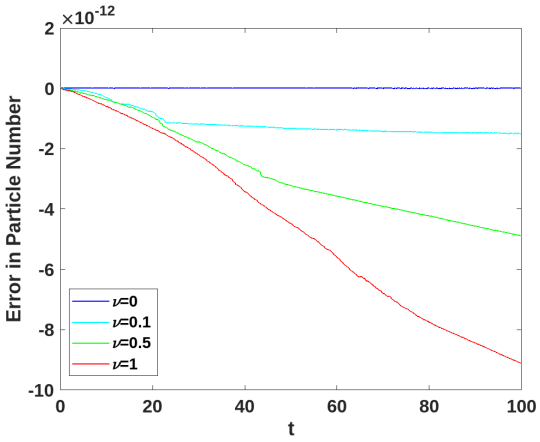

(b) Total particle number. IMEX.

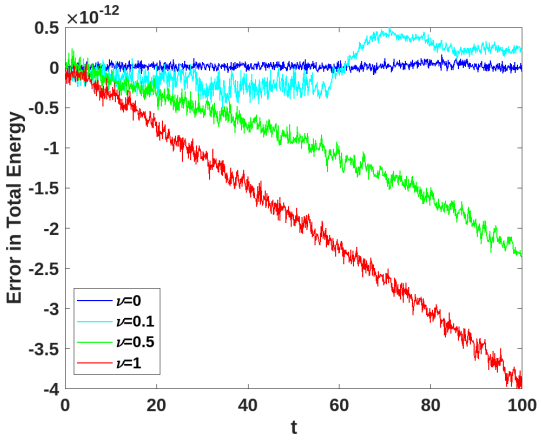

(c) Total energy. Explicit.

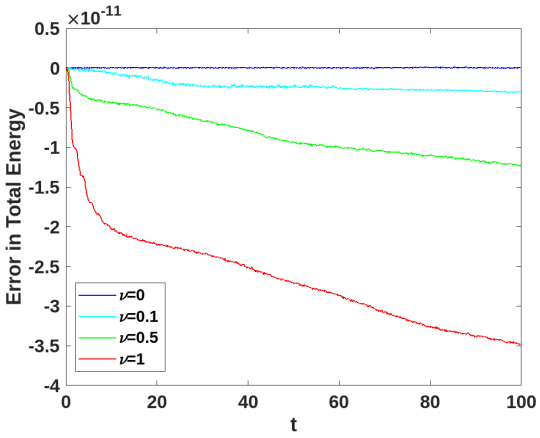

(d) Total energy. IMEX.

Figure 4.3: Two stream instability in Example 4.4. Evolution of the relative error in total particle number (top) and total energy (bottom) by the explicit scheme (left) and the IMEX scheme (right). 50×100 mesh.

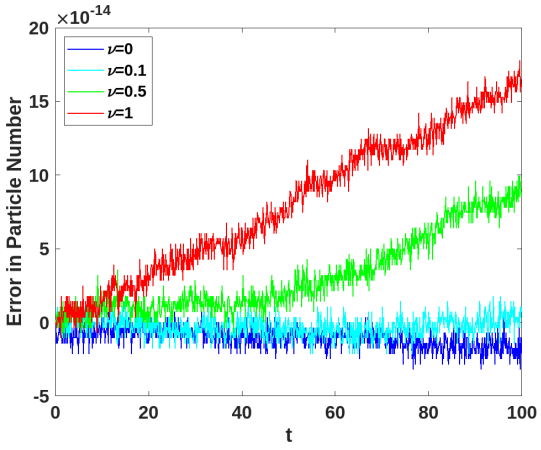

(a) Total particle number. Explicit.

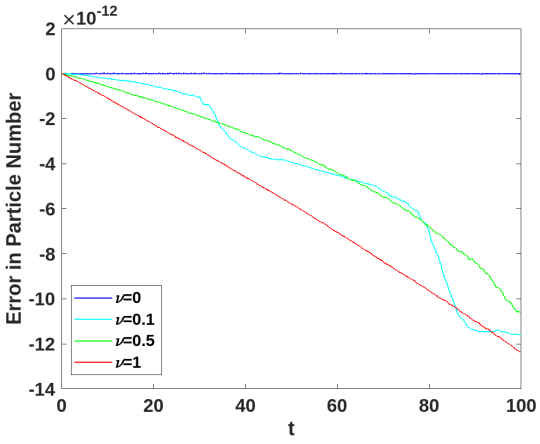

(b) Total particle number. IMEX.

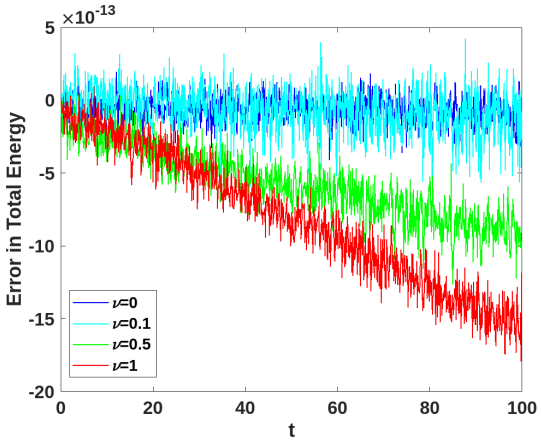

(c) Total energy. Explicit.

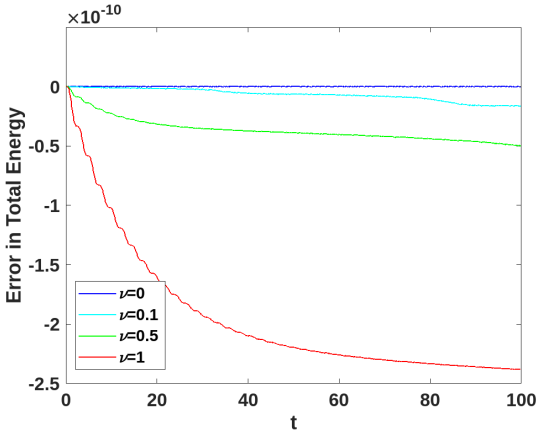

(d) Total energy. IMEX.

Figure 4.4: Bump-on-tail instability in Example 4.5. Evolution of the relative error in total particle number (top) and total energy (bottom) by the explicit scheme (left) and the IMEX scheme (right). 50×100 mesh.

phenomenon arises due to long time simulation of numerical methods. It was shown in [24] that piece-wise constant approximations in velocity space lead to a recurrence phenomenon. Such behavior was also seen in numerical simulations for weak Landau damping in[R2] [35, 63] and for strong Landau damping in [62].[R2] For both weak and strong Landau damping, the damping rate decreases as $\nu > 0$ increases. The enstrophy and the entropy with $\nu > 0$ stabilizes to a steady state faster than the case of $\nu = 0$. Figure 4.6 plots the electric energy for two-stream instability and bump-on-tail instability. [R2]

Figures 4.7 and 4.8 plot contours of f for two-stream instability with $\nu = 1$ and $\nu = 0.001$, respectively. Figures 4.9 and 4.10 plot contours of f for bump-on-tail instability with $\nu = 1$ and $\nu = 0.001$. It can be observed that for large collision frequencies such as $\nu = 1$, the solution rapidly reaches a steady state (equilibrium or Maxwellian distribution) in the velocity direction regardless of the Vlasov component, while for small collision frequencies such as $\nu = 0.001$, the behavior of the solution resembles the $\nu = 0$ scenario documented in [9]. However, as time goes by, the solution eventually converges to a Maxwellian distribution. Overall, the introduction of the DFP operator drives solutions towards a steady state, exhibiting a Maxwellian distribution along the v-axis.

5 Conclusion

In this paper, we have developed energy-conserving numerical schemes for solving the VA system coupled with the DFP collision operator. We have introduced two energy-conserving temporal discretization methods, a second-order explicit scheme and a second-order IMEX scheme, coupling with the DG methods for the phase space, to achieve the total particle number and total energy conservation at the fully discrete level. Additionally, we have proven the L^2 stability of the fully discrete explicit scheme. Numerical experiments have been conducted to demonstrate the performance of ~~the~~[R2] the proposed schemes. Further research includes exploring their extension to ~~more complex plasma models and specific phenomena~~[R2] high dimensional systems and designing numerical schemes that have the entropy decay structure.[R2].

Acknowledgments

Research work of J. Hu was partially supported by AFOSR grant FA9550-21-1-0358 and DOE grant DE-SC0023164. Research work of C.-W. Shu was partially supported by NSF grant DMS-2309249. Research work of X. Zhong was partially supported by the NSFC Grant 12272347.

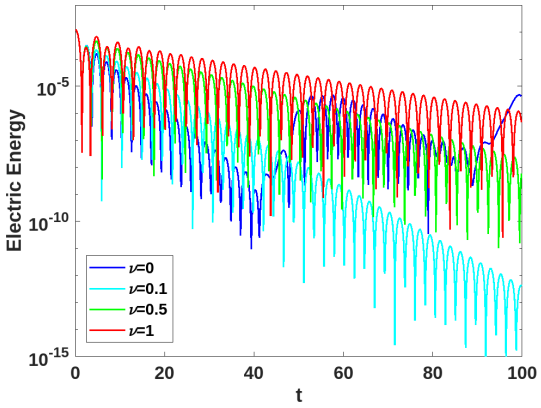

(a) Weak Landau damping. Electric energy.

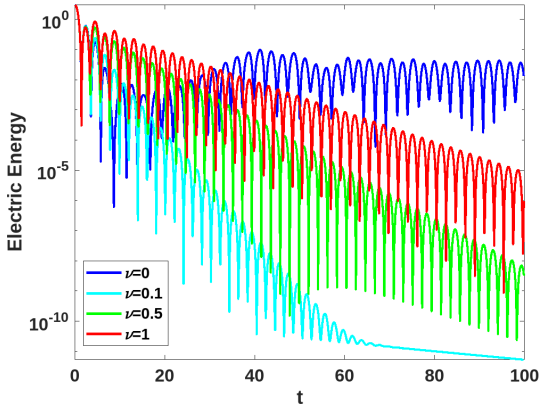

(b) Strong Landau damping. Electric energy.

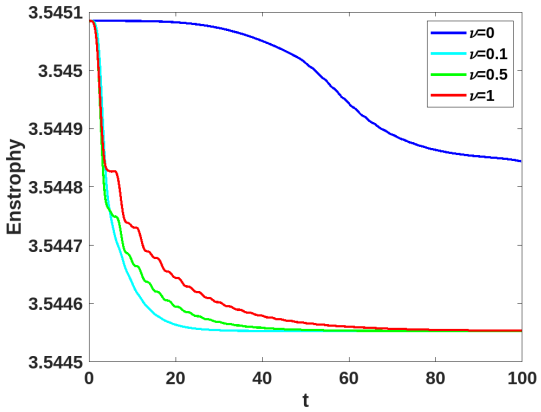

(c) Weak Landau damping. Enstrophy.

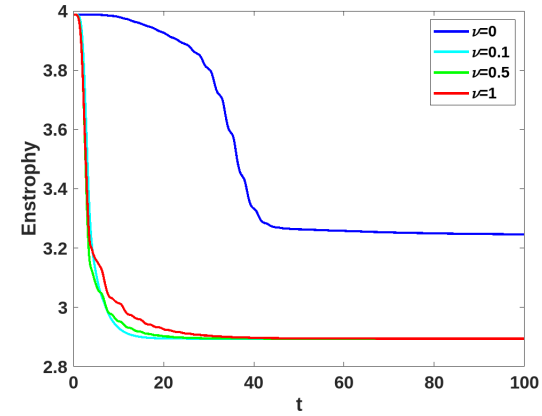

(d) Strong Landau damping. Enstrophy.

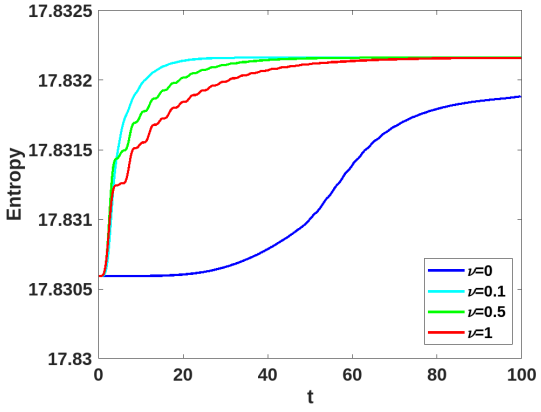

(e) Weak Landau damping. Entropy.

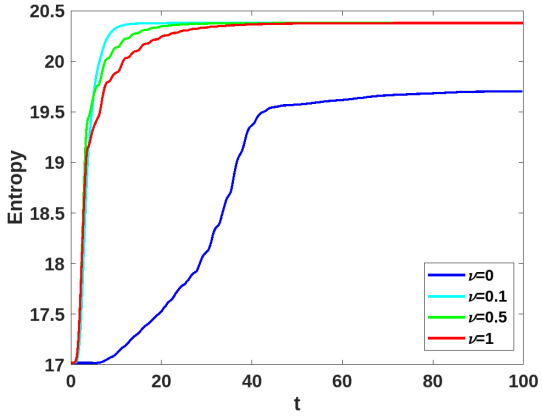

(f) Strong Landau damping. Entropy.

Figure 4.5: The electric energy (top), the enstrophy (middle), and the entropy (bottom) for weak Landau damping (left) and strong Landau damping (right) of Example 4.3. Explicit scheme. 50×100 mesh.

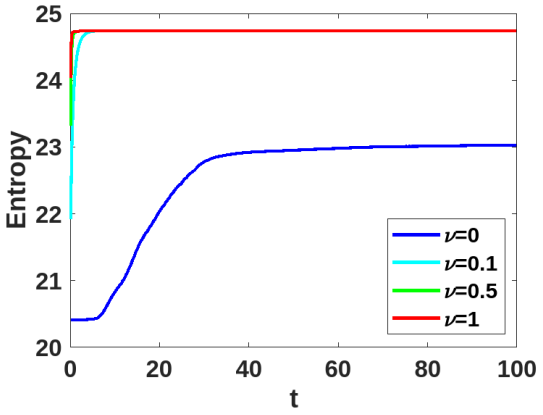

(a) Two stream instability. Entropy.

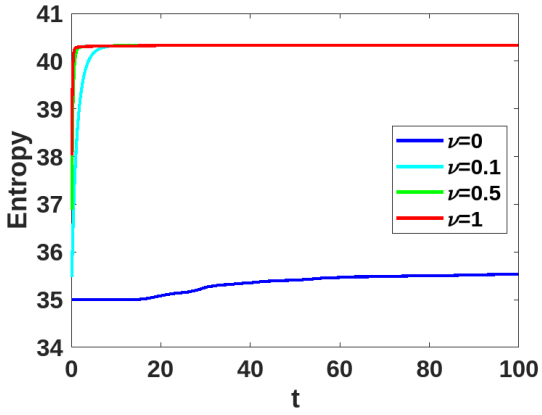

(b) Bump-on-tail instability. Entropy.

Figure 4.6: The entropy for two stream instability of Example 4.4 (left) and bump-on-tail instability (right) of Example 4.5. Explicit scheme. 50×100 mesh.[R2]

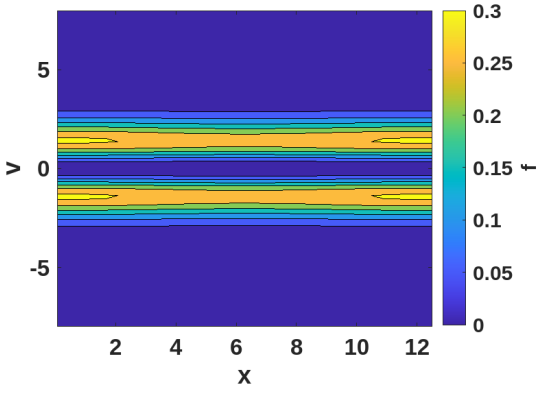

(a) t=0.

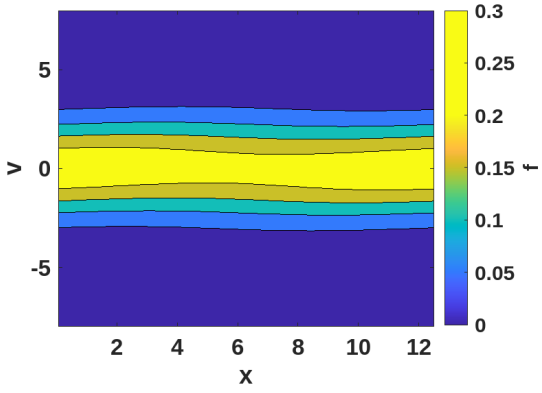

(b) t=1.

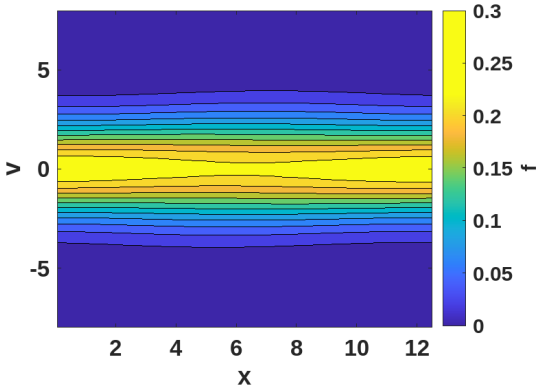

(c) t=2.

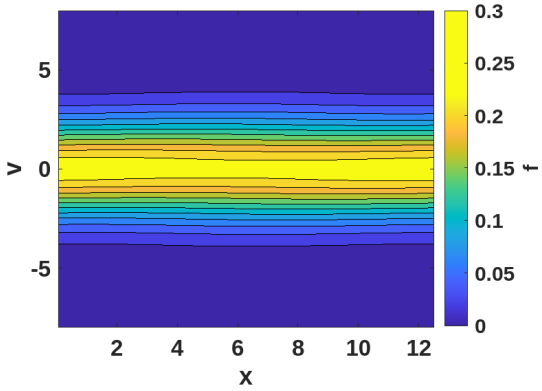

(d) t=5.

Figure 4.7: Phase space contour plots for two-stream instability in Example 4.4 at the indicated time. Explicit scheme. $\nu = 1$. 50×100 mesh.

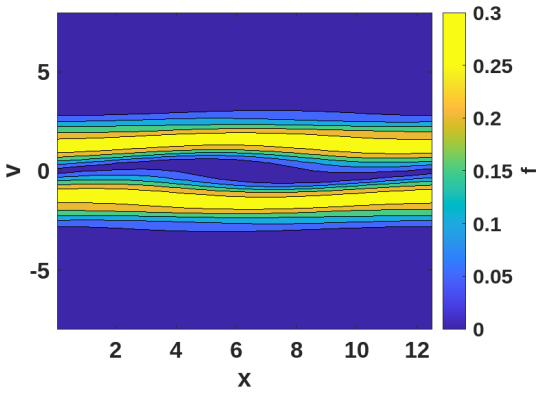

(a) t=10.

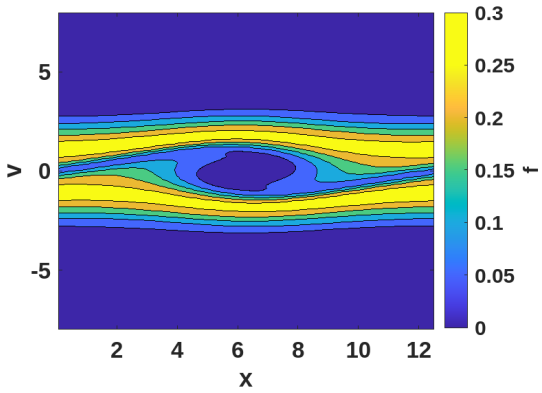

(b) t=15.

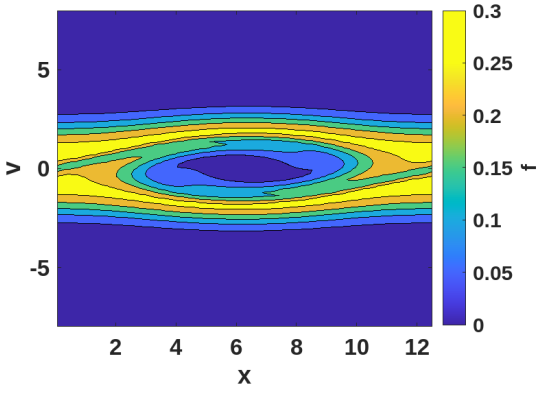

(c) t=20.

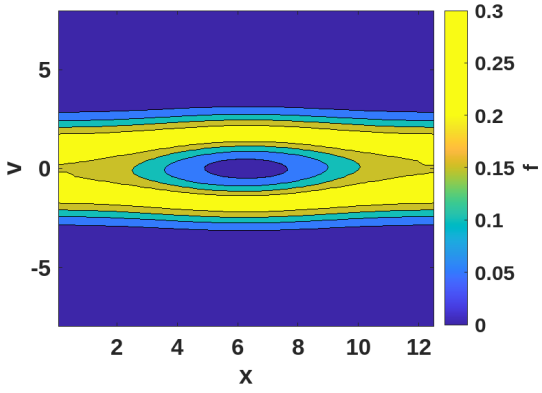

(d) t=40.

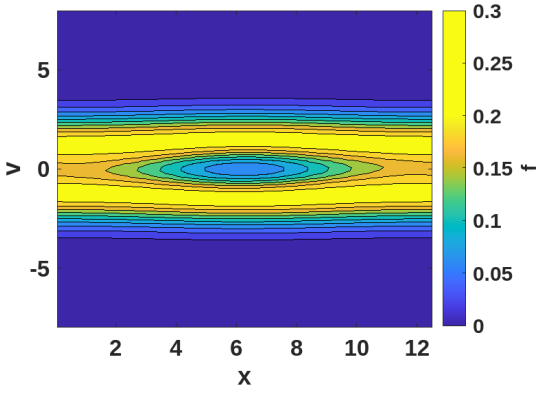

(e) t=80.

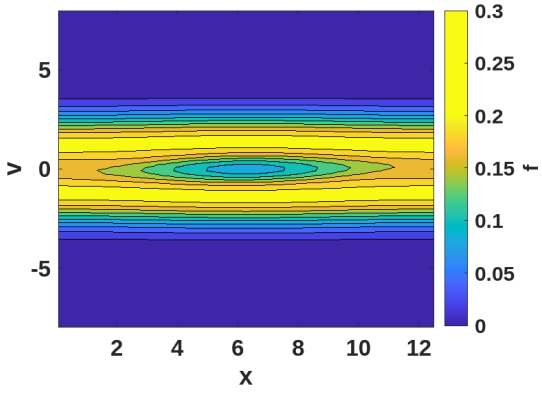

(f) t=100.

Figure 4.8: Phase space contour plots for two-stream instability in Example (4.4) at the indicated time. Explicit scheme. $\nu = 0.001$. 50×100 mesh.

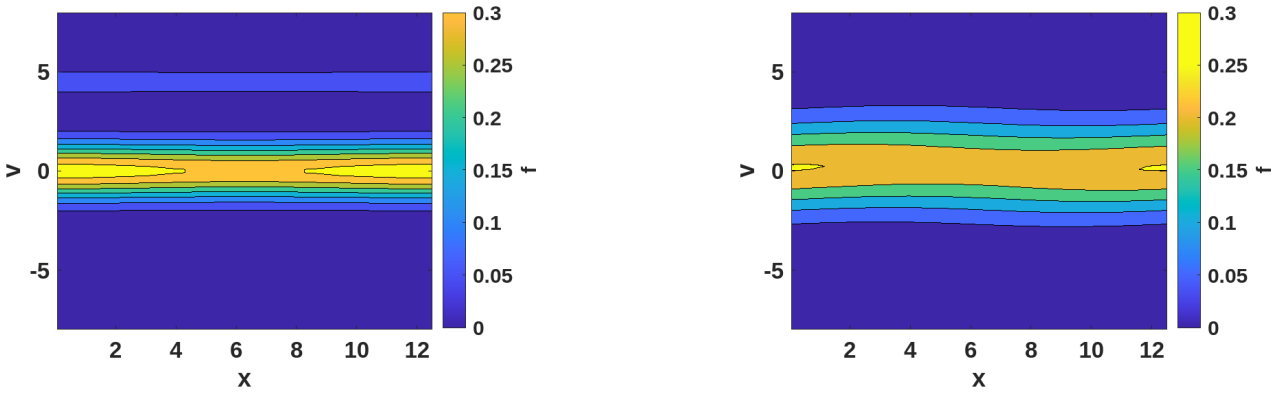

(a) t=0.

(b) t=1.

(c) t=2.

(d) t=5.

Figure 4.9: Phase space contour plots for bump-on-tail instability in Example 4.5 at the indicated time. Explicit scheme. $\nu = 1$. 50×100 mesh.

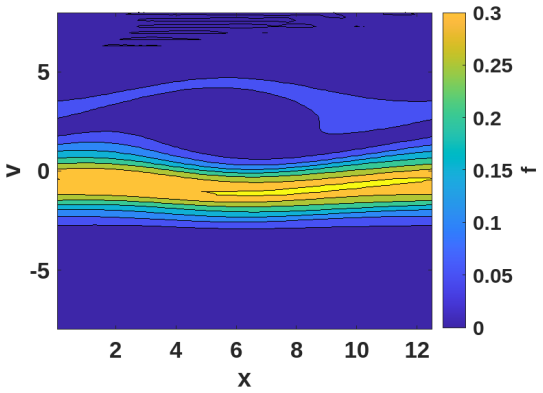

(a) t=15.

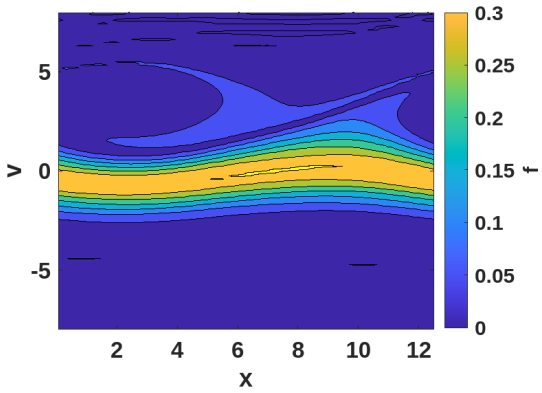

(b) t=20.

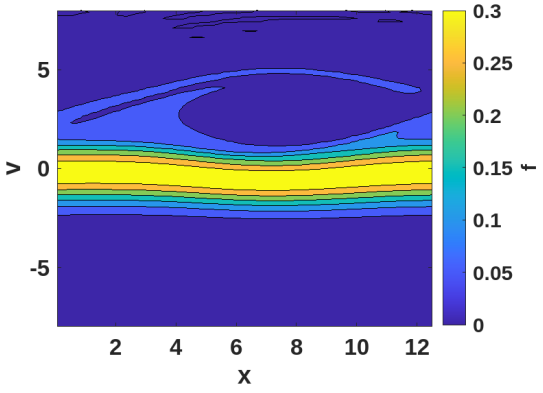

(c) t=30.

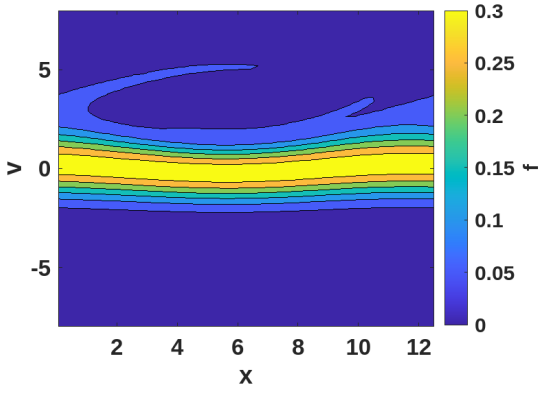

(d) t=50.

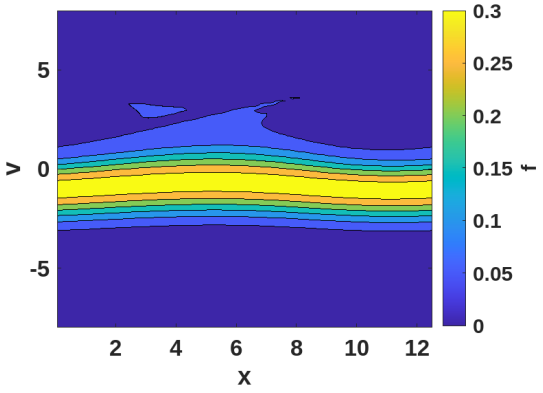

(e) t=60.

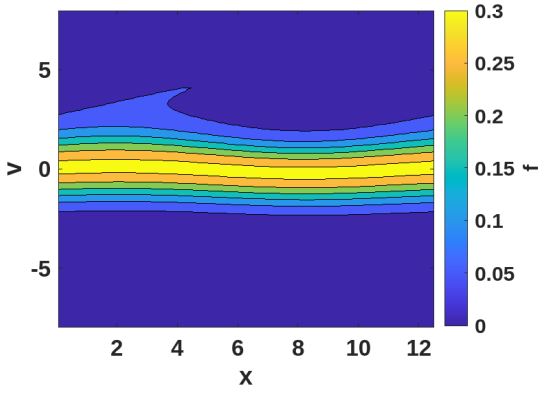

(f) t=100.

Figure 4.10: Phase space contour plots for bump-on-tail instability in Example 4.5 at the indicated time. Explicit scheme. $\nu = 0.001$. 50×100 mesh.

References

[1] I. Almuslimani and N. Crouseilles. Conservative stabilized Runge-Kutta methods for the Vlasov-Fokker-Planck equation. *J. Comput. Phys*, 488:112241, 2023.

[2] M. Asadzadeh and P. Kowalczyk. Convergence analysis of the streamline diffusion and discontinuous Galerkin methods for the Vlasov-Fokker-Planck system. *Numer. Methods Partial Differ. Equ.*, 21:472–495, 2004.

[3] B. Ayuso, J. Carrillo, and C.-W. Shu. Discontinuous Galerkin methods for the one-dimensional Vlasov–Poisson system. *Kinet. Relat. Models*, 4:955–989, 2011.

[4] B. Ayuso, J. Carrillo, and C.-W. Shu. Discontinuous Galerkin methods for the multi-dimensional Vlasov–Poisson problem. *Math. Models Methods Appl. Sci.*, 22 (12):1140–1174, 2012.

[5] N. Besse, E. Deriaz, and E. Madaule. Adaptive multiresolution semi-Lagrangian discontinuous Galerkin methods for the Vlasov equations. *J. Comput. Phys.*, 332:376–417, MAR 1 2017.

[6] C. Birdsall and A. Langdon. Plasma physics via computer simulation. *IOP Publishing*, 1991.

[7] G. Chen, L. Chacón, and D. Barnes. An energy-and charge-conserving, implicit, electrostatic particle-in-cell algorithm. *J. Comput. Phys.*, 230 (18):7018–7036, 2011.

[8] C. Cheng and G. Knorr. The integration of the Vlasov equation in configuration space. *J. Comput. Phys.*, 22 (3):330–351, 1976.

[9] Y. Cheng, A. J. Christlieb, and X. Zhong. Energy-conserving discontinuous Galerkin methods for the Vlasov-Ampere system. *J. Comput. Phys.*, 256:630–655, 2014.

[10] Y. Cheng, A. J. Christlieb, and X. Zhong. Energy-conserving discontinuous Galerkin methods for the Vlasov–Maxwell system. *J. Comput. Phys.*, 279:145–173, 2014.

[11] Y. Cheng, A. J. Christlieb, and X. Zhong. Energy-conserving numerical simulations of electron holes in two-species plasmas. *Eur. Phys. J. D*, 69(3):67, 2015.

[12] Y. Cheng, A. J. Christlieb, and X. Zhong. Numerical study of the two-species Vlasov–Ampère system: energy-conserving schemes and the current-driven ion-acoustic instability. *J. Comput. Phys.*, 288:66–85, 2015.

[13] Y. Cheng, I. Gamba, and P. Morrison. Study of conservation and recurrence of Runge–Kutta discontinuous Galerkin schemes for Vlasov–Poisson systems. *J. Sci. Comput.*, 56:319–349, 2013.

[14] Y. Cheng, I. M. Gamba, F. Li, and P. J. Morrison. Discontinuous Galerkin Methods for the Vlasov–Maxwell Equations. *SIAM J Numer Anal*, 52(2):1017–1049, 2014.

[15] Y. Cheng, I. M. Gamba, A. Majorana, and C.-W. Shu. A brief survey of the discontinuous Galerkin method for the Boltzmann–Poisson equations. *SeMA J.*, 54:47–64, 2011.

[16] P. G. Ciarlet. *The Finite Element Method for Elliptic Problems.* Classics in Applied Mathematics. Society for Industrial and Applied Mathematics (SIAM), Philadelphia, PA, 2002.

[17] B. Cockburn, S. Hou, and C.-W. Shu. The Runge-Kutta local projection discontinuous Galerkin finite element method for conservation laws. IV: The multidimensional case. *Math. Comput.*, 54:545–581, 1990.

[18] B. Cockburn, G. Karniadakis, and C.-W. Shu. *Discontinuous Galerkin Methods: Theory, Computation and Applications*, volume 11 of *Lecture Notes in Computational Science and Engineering, Part I.* Springer, 2000.

[19] B. Cockburn, S. Lin, and C.-W. Shu. TVB Runge-Kutta local projection discontinuous Galerkin finite element method for conservation laws. III: One dimensional systems. *J. Comput. Phys.*, 84:90–113, 1989.

[20] B. Cockburn and C.-W. Shu. TVB Runge-Kutta local projection discontinuous Galerkin finite element method for conservation laws II: general framework. *Mathematics of Computation*, 52(186):411–435, 1989.

[21] B. Cockburn and C.-W. Shu. The local discontinuous Galerkin method for time-dependent convection-diffusion systems. *SIAM J Numer Anal*, 35(6):2440–2463, 1998.

[22] N. Crouseilles and T. Respaud. A charge preserving scheme for the numerical resolution of the Vlasov–Ampère equations. *Commun. Comput. Phys.*, 10:1001–1026, 2011.

[23] J. Dougherty. Model Fokker-Planck equation for a plasma and its solution. *Phys. Fluids*, 7:1788–1799, 1964.

[24] L. Einkemmer and A. Ostermann. Convergence analysis of a discontinuous galerkin/strang splitting approximation for the vlasov–poisson equations. *SIAM Journal on Numerical Analysis*, 52(2):757–778, Jan. 2014.

[25] N. Elkina and J. Büchner. A new conservative unsplit method for the solution of the Vlasov equation. *Commun. Comput. Phys.*, 213 (2):862–875, 2006.

[26] E. Endeve and C. Hauck. Conservative DG method for the micro-macro decomposition of the Vlasov-Poisson-Lenard-Bernstein model. *J. Comput. Phys.*, 462, 2022.

[27] J. Eshaghi, H.Adibi, and S.Kazem. On a numerical investigation of the time fractional Fokker- Planck equation via local discontinuous Galerkin method. *Int. J. Comput. Math.*, 94, 2017.

[28] E. Fijalkow. A numerical solution to the Vlasov equation. *Comput. Phys. Commun.*, 116:319–328, 1999.

[29] F. Filbet, E. Sonnendrücker, and P. Bertrand. Conservative numerical schemes for the Vlasov equation. *J. Comput. Phys.*, 172:166–187, 2001.

[30] M. Francisquez, J. Juno, A. Hakim, G. Hammett, and D. Ernst. Improved multispecies Dougherty collisions. *J. Plasma Phys.*, 88, 2022.

[31] S. Gottlieb, C.-W. Shu, and E. Tadmor. Strong stability-preserving high-order time discretization methods. *SIAM Rev.*, 43:89–112, 2001.

[32] A. Hakim, M. Francisquez, J. Juno, and G. Hammett. Conservative discontinuous Galerkin schemes for nonlinear Dougherty-Fokker-Planck collision operators. *J. Plasma Phys.*, 86:905860403, 2020.

[33] R. Heath. Numerical analysis of the discontinuous Galerkin method applied to plasma physics. *Ph.D. dissertation, University of Texas at Austin*, 79:184–199, 2007.

[34] R. Heath, I. Gamba, P. Morrison, and C. Michler. A discontinuous Galerkin method for the Vlasov–Poisson system. *J. Comput. Phys.*, 231(4):1140–1174, 2012.

[35] A. Ho, I. A. M. Datta, and U. Shumlak. Physics-based-adaptive plasma model for high-fidelity numerical simulations. *Frontiers in Physics*, 6:105, Sept. 2018.

[36] R. Hockney and J. Eastwood. *Computer Simulation Using Particles*. McGraw-Hill, 1981.

[37] J. Hu and X. Zhang. On a class of implicit-explicit Runge Kutta schemes for stiff kinetic equations preserving the Navier-Stokes limit. *J. Sci. Comput.*, 73:797–818, 2017.

[38] S. Jin and B. Yan. A class of asymptotic-preserving schemes for the Fokker-Planck-Landau equation. *J. Comput. Phys.*, 230:6420–6437, 2011.

[39] A. Klimas. A method for overcoming the velocity space filamentation problem in collisionless plasma model solutions. *J. Comput. Phys.*, 68:202–226, 1987.

[40] A. Klimas and W. Farrell. A splitting algorithm for Vlasov simulation with filamentation filtration. *J. Comput. Phys.*, 110:150–163, 1994.

[41] L. D. Landau. The kinetic equation in the case of Coulomb interaction. *Zh. Eksper. i Teoret. Fiz.*, 7:203–209, 1937.

[42] A. Lenard and I. Bernstein. Plasma oscillations with diffusion in velocity space. *Phys. Rev.*, 112(5):1456–1459, 1958.

[43] H. Liu, X. Cai, Y. Cao, and G. Lapenta. An efficient energy conserving semi-Lagrangian kinetic scheme for the Vlasov-Ampère system. *J. Comput. Phys.*, 492:112412, 2023.

[44] E. Madaule, M. Restelli, and E. Sonnendruecker. Energy conserving discontinuous Galerkin spectral element method for the Vlasov-Poisson system. *J. Comput. Phys.*, 279:261–288, DEC 15 2014.

[45] S. Markidis and G. Lapenta. The energy conserving particle-in-cell method. *J. Comput. Phys.*, 230(18):7037–7052, 2011.

[46] J.-M. Qiu and A. J. Christlieb. A conservative high order semi-Lagrangian WENO method for the Vlasov equation. *J. Comput. Phys.*, 229 (4):1130–1149, 2010.

[47] J.-M. Qiu and C.-W. Shu. Positivity preserving semi-Lagrangian discontinuous Galerkin formulation: Theoretical analysis and application to the Vlasov–Poisson system. *J. Comput. Phys.*, 230 (23):8386–8409, 2011.

[48] J. Rossmanith and D. Seal. A positivity-preserving high-order semi-Lagrangian discontinuous Galerkin scheme for the Vlasov–Poisson equations. *J. Comput. Phys.*, 230 (16):6203–6232, 2011.

[49] T. Sommerer, W. Hitchon, R. Harvey, and J. Lawler. Self-consistent kinetic calculations of helium rf glow discharges. *Phys. Rev. A*, 43:4452–4472, 1991.

[50] T. Sommerer, W. Hitchon, and J. Lawler. Electron heating mechanisms in helium rf glow discharges: A self-consistent kinetic calculation. *Phys. Rev. Lett.*, 63:2361–2364, 1989.

[51] T. Sommerer, W. Hitchon, and J. Lawler. Self-consistent kinetic model of the cathode fall of a glow discharge. *Phys. Rev. A*, 39:6356–6366, 1989.

[52] E. Sonnendrücker, J. Roche, P. Bertrand, and A. Ghizzo. The semi-Lagrangian method for the numerical resolution of the Vlasov equation. *J. Comput. Phys.*, 149 (2):201–220, 1999.

[53] W. Taitano, D. Knoll, and L. Chacón. Charge-and-energy conserving moment-based accelerator for a multi-species Vlasov–Fokker–Planck–Ampère system, part II: Collisional aspects. *J. Comput. Phys.*, 284:737–757, 2015.

[54] P. Ulbl, D. Michels, and F. Jenko. Implementation and verification of a conservative, multi-species, gyro-averaged, full-f, Lenard-Bernstein/Dougherty collision operator in the gyrokinetic code GENE-X. *Contrib. to Plasma Phys.*, 62, 2021.

[55] Y. Wang, J. Zhang, and G. Ni. A gas-kinetic scheme for collisional Vlasov-Poisson equations in cylindrical coordinates. *Commun. Comput. Phys.*, 32(3):779–809, June 2022.

[56] D. Yi and S. Bu. A mass conservative scheme for solving the Vlasov–Poisson equation using characteristic curve. *J. Comput. Appl. Math.*, 324:1–16, 2017.

[57] T. Yin, X. Zhong, and Y. Wang. Highly efficient energy-conserving moment method for the multi-dimensional Vlasov-Maxwell system. *J. Comput. Phys.*, 475:111863, 2023.

[58] S. Zaki, L. Gardner, and T. Boyd. A finite element code for the simulation of one-dimensional Vlasov plasmas. I. Theory. *J. Comput. Phys.*, 79:184–199, 1988.

[59] S. Zaki, L. Gardner, and T. Boyd. A finite element code for the simulation of one-dimensional Vlasov plasmas. II. Applications. *J. Comput. Phys.*, 79:200–208, 1988.

[60] C. Zhang and I. Gamba. A conservative scheme for Vlasov Poisson Landau modeling collisional plasmas. *J. Comput. Phys.*, 340:470–497, 2017.

[61] Q. Zhang and F. Gao. A fully-discrete local discontinuous Galerkin method for convection-dominated Sobolev equation. *J. Comput. Phys*, 51(1):107–134, Apr. 2012.

[62] N. Zheng, X. Cai, J.-M. Qiu, and J. Qiu. A conservative semi-lagrangian hybrid hermite weno scheme for linear transport equations and the nonlinear vlasov–poisson system. *SIAM Journal on Scientific Computing*, 43(5):A3580–A3606, Jan. 2021.

[63] T. Zhou, Y. Guo, and C.-W. Shu. Numerical study on Landau damping. *Physica D*, 157 (4):322–333, 2001.